Slag Properties in the Primary Production Process of Mn-Ferroalloys

MERETE TANGSTAD, SERGEY BUBLIK, SHOKOUH HAGHDANI, KRISTIAN ETIENNE EINARSRUD, and KAI TANG

The thermodynamic and kinetic properties of the carbothermic reduction of MnO in the five-component slag, MnO-SiO_2-CaO-MgO-Al_2O_3, is critical in the production process of Mn-ferroalloys. While the reduction rate is mainly dependent on the presence of a solid MnO phase in the slag for Mn-Fe-alloys, the rate for the Mn-Si-Fe alloys has two distinct steps, a slow step followed by a fast step. The extent of the slow step has been shown to be dependent on the S content in the slag. The thermo-physical properties of viscosity, density, interfacial tension and electrical resistivity is reviewed, and these properties are mainly determined by the total basicity.

I. OVERVIEW OF THE MN-ALLOY PRODUCTION PROCESS

MN-FERROALLOYS are alloys containing mostly Mn, Fe, Si and C. Manganese is the main element and typically accounts for between 60 and 80 wt pct of the alloy. Iron will always follow the raw materials and practically all iron in the raw materials will end up in the alloy. Silicon may be less than 1 pct or up to 30 pct. Less than 1 pct Si is usually called FeMn (ferromanganese) and alloys with 16 to 30 pct is called SiMn (silicomanganese). The metal will be saturated with carbon from the furnace and will be 7 pct C for FeMn and for SiMn the carbon content is dependent on the amount of silicon. Typically, for 18 pct Si the carbon content is less than 2 pct C. As for most reduction processes, the metal composition is determined by the slag properties, and the slag in the Mn-ferroalloy will mainly be MnO, SiO_2, MgO, CaO and Al_2O_3 as all the iron ends up in the metal. There are a number of definitions of slag basicity that can be used to describe the composition of the slag. In this paper, the basicity will be given as $B = \frac{CaO+MgO}{SiO_2+Al_2O_3}$. Trace elements are counted as basic or acid oxides, depending on their nature.

The temperatures in the closed Mn-ferroalloy furnaces can be from 200 °C to 600 °C on the top of the charge to 1500 °C to 1600 °C in the tapped slag. This means that in upper part of the furnace, the low temperature zone, the raw materials will be solid, and when it enters the area on top of the coke-bed, around 1200 °C to 1400 °C, the raw materials will melt into a primary slag. This slag will coexist with the solid carbon materials added to the furnace (Figure 1). This paper will discuss the knowledge we have on MnO-slags related to the primary production of FeMn or SiMn inside the Submerged Arc Furnace. First we will discuss the mechanism of slag formation, the thermodynamics, and the kinetics. Next, a summary of key slag properties is presented. These key properties include the MnO slag structure, viscosity, density, interfacial tension and wetting properties, and electrical conductivity. The pathway of the slag considered in this work will start with the production of a primary slag from the raw materials, followed by the reduction of valuable elements into a Mn-alloy and finally the drainage, or tapping, from the furnace.

Most of the slag will as discussed later, follow the increasing temperature. Some slag may however be circulated into the low temperature area. In Mn-alloy production, slags have been known to be sputtered up to the cold furnace top from the high temperature area as seen in Figure 2.[2,3] This is believed to happen if the permeability of the charge is poor, and the raw materials are not heated gradually, or if too violent foaming of the slag occurs.

MERETE TANGSTAD, SERGEY BUBLIK, SHOKOUH HAGHDANI, KRISTIAN ETIENNE EINARSRUD are with the Department of Material Science and Engineering, Norwegian University of Science and Technology, 7491 Trondheim, Norway. Contact e-mail: Merete.Tangstad@ntnu.no KAI TANG is with the SINTEF Industry, SINTEF, 7465 Trondheim, Norway.
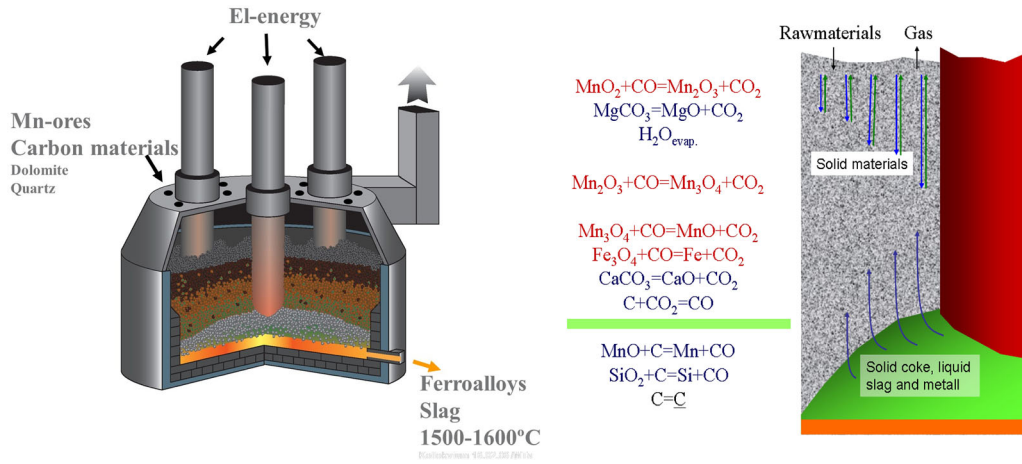
Fig. 1—Overview of a typical closed furnace producing Mn-alloys (left) and an illustration of zones and reactions around one of the electrodes (right).[1] (Figure is reprinted with permission from Ref. 1).
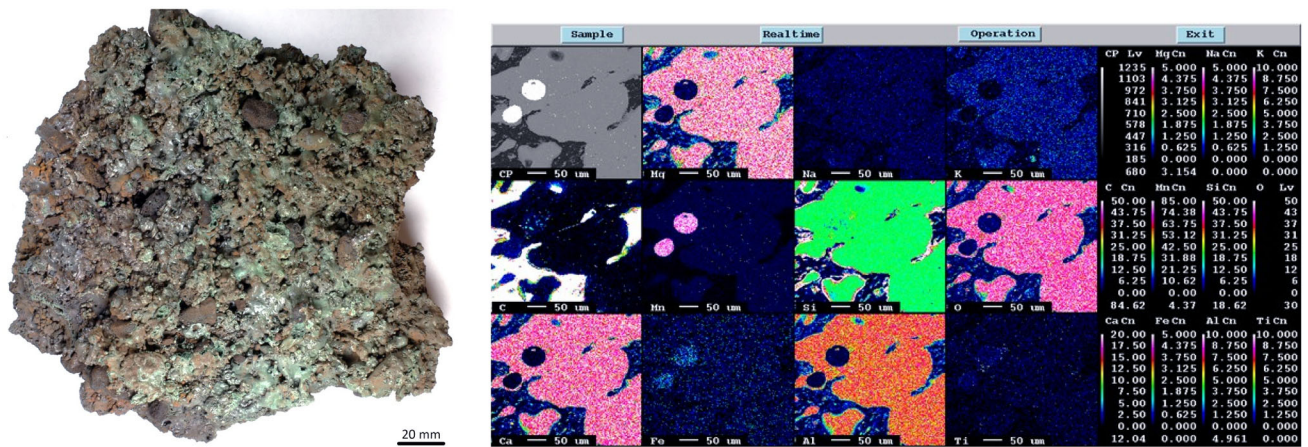

Fig. 2—Slag infiltrated charge sample at top of the furnace charge taken from a FeMn furnace (left picture) showing low alkali binder phase (right)[4].

II. MELTING OF ORES AND REDUCTION OF PRIMARY SLAGS

The melting of the raw materials to a primary slag and the following reduction to Mn-ferroalloys are closely related. It is hence appropriate to start with the Mn-bearing raw materials and the primary slag it produces at around 1200 °C and up. Table I show some typical ores, where the metallurgical grade ore typically have more than 35 pct Mn. After being heated in solid state in the prereduction zone, all higher manganese (MnO_2, Mn_2O_3 and Mn_3O_4) has been reduced to MnO, the iron oxides are reduced to metallic phase, and all the carbonates ($CaCO_3$, $MgCO_3$, $MnCO_3$) are decomposed to basic oxides (CaO, MgO and MnO). The main elements in the oxide phase will now be the 5 components MnO-SiO_2-Al_2O_3-CaO-MgO. Table II shows the chemical composition calculated from the chemical analyses of the ore of the primary slag. It can be noted that there will also be a number of trace elements like TiO_2, K_2O, BaO, however these will not be discussed further here.

The five-component pre-reduced Mn-ores, typically containing around 70 pct MnO, will as it melts down dissolve fluxes. The fluxes can typically be "pre-reduced" limestone or dolomite or quartz and reduced MnO-slags if SiMn is produced. In the liquid (or partly liquid) state , the MnO and SiO_2 may be reduced to metallic Mn-Fe-Si-$C_{saturated}$ alloy according to reactions [1] and [2], where the parentheses denote a slag phase and underscored denotes metallic phases. The carbon can be solid carbon, *i.e.,* coke particles, or carbon dissolved in the metal. Some of the MnO and SiO_2 still will remain in the slag, and the tapped slag will thus be the same 5-component slag containing MnO, SiO_2, Al_2O_3, CaO and MgO.
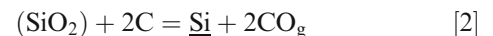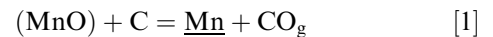
$$(MnO) + C = \underline{Mn} + CO_g \qquad [1]$$

$$(SiO_2) + 2C = \underline{Si} + 2CO_g \qquad [2]$$

Table I. Typical Analyses of Mn-Ores[1,5,6]

Manganese Ore		Mn	Fe	SiO2	Al2O3	MgO	CaO	P	CO2
Comilog MMA	Gabon	50.5	2.7	4.0	5.5	0.3	0.2	0.11	0.1
Comilog Sinter		58.5	3.5	7.0	6.5	0.0	0.1	0.12	0.0
Mn-Nodules	Mexico	37.7	7.9	14.9	3.9	8.1		0.085	
Asman 48	South Africa	51.3	10.1	5.5	0.4	0.7	4.3	0.04	0.8
Mamatwan		37.8	4.6	4.0	0.5	3.5	14.7	0.02	17.0
Gloria		39.1	5.0	5.7	0.3	3.8	12.7	0.02	15.4
Wessel 38 pct		42.3	13.2	4.9	2.5	1.0	6.0	0.04	3.6
Wessel 50 pct		50.2	10.0	3.6	0.4	1.0	5.6	0.04	2.6
Groote Eylandt	Australia	48.8	4.2	6.9	4.2	0.1	0.1	0.09	0.5
Amapa Sinter	Brazil	49.1	9.6	7.6	7.6	0.5	0.8	0.10	0.0
Amapa Miudo 40		41.3	12.5	5.9	8.1	0.1	0.3	0.11	3.5
CVRD Sinter		54.5	4.7	5.4	8.7	0.5	1.9	0.11	0.2
CVRD Lump		45.0	4.7	2.6	8.6	0.2	0.2	0.09	14.4
Nikopol-Oxide	Ukraine	29–43	1–3	11–24	1.4–3.3	0.8–2	4–10	0.15–0.3	
Nikopol-Pyrolusite		47.5	0.65	8.6	1.6	0.6	2	0.2	
Nikopol-Carbonate		22–28	1.5–3	13–16	1.7–2.3	1.5–2.2	7–13	0.3–0.6	
Tchiatura-Oxide	Georgia	30–44	0.7–4	6–17	1.3–2.6	1–2.5	3.8–5.5	0.1–0.4	
Tchiatura-Pyrolusite		28	1.3	17.6	2.9	1.5	8.2	0.2	
Tchiatura-carbonate		23–25	1.3	16–17	2	2.5	10	0.15	
Zapadny Kamys	Kazakhstan	17–19	5–6	40–42	5–6.5	1–1.5	1.2–1.7	0.035	

A number of industrial-, and pilot scale- tap-slag composition have been reported. For FeMn slags the MnO content varies from 15 to 40 wt pct depending on the basicity.[1,5,7–12] High basicity charges, that is basicities above 1.1, typically have less than 25 pct MnO. Basicities around 0.7 typically has 35-40 pct MnO, and this is close to the liquidus line at 1500 °C, which is reported to be close to the tapping temperature.[13] Some smaller furnaces, *e.g.*, a 21 MVA furnace,[9] show an MnO content as low as 19 pct MnO with a basicity of 0.9, and it is speculated if smaller furnaces may produce lower MnO contents. Acid slags with a basicity 0.2-0.3 will also tap at about 40 pct MnO.

For SiMn slags a typical Si content is 15-18 pct Si, and to obtain this around 40 pct SiO$_2$ is needed in the slag. Industrially, less than 20 pct MnO is remaining in the slag, and it can be down to 5-10 pct. In pilot scale operation the MnO content in SiMn slags are typically seen to be a bit higher than the industrial slags, that is up to 25 pct MnO.[1,5,14–19]

To sum this up, FeMn charges will be reduced from a primary slag with more than 60 pct MnO to 15 to 40 pct MnO in the tapped slag, while SiMn charge mixes is reduced from a primary slag with more than 35 pct MnO (as the Mn-sources are mixed with both fluxes and quartz) to around 10 pct MnO tapped at 1600 °C.[16]

The slag composition will of course be affected by the temperature. Due to reported tapping temperatures of around 1500 °C for FeMn[13] and 1600 °C for SiMn tappings,[16] one assumes that this can also be the temperatures inside the high temperature zones in the furnaces. As the temperatures are varying both due to the electrode paths in the furnace, given by the coke-bed size and shape, and raw material properties, the temperature in the high temperature zone will vary both in space and in time.

A. Phase Composition in Mn-Slags and Melting Behaviour Of Ores.

The melting behaviour of the above described 5 component system can be simplified to the MnO-SiO$_2$ system where "MnO" in reality represents the basic oxides MnO, CaO, and MgO and "SiO$_2$" represent the acid oxides SiO$_2$ and Al$_2$O$_3$ as illustrated in Figure 3. Although Al$_2$O$_3$ is an amphoteric oxide, it will for manganese slags behave as an acidic oxide, though less acid in more acid SiMn slags *vs.* more basic FeMn slags.[16,20]

For FeMn slags, containing a high amount of MnO, the reduction will start when a liquid phase is present in the material that is above the solidus, represented by the 1306 °C horizontal line in Figure 3. The reduction may hence start in the area of 1300 °C according to the equilibrium state. At this point, the reduction starts and hence it is believed that the endothermic reaction (reaction [1]) will consume more energy and hence the heating rate will decrease drastically. The reduction will go through a two-phase area, and the primary slag will consist of a liquid with a solid MnO phase as seen in Figure 4. The presence of a solid MnO phase has two major consequences; first it will have a high impact on the activity of MnO and secondly it will have a large effect on the flow properties (*i.e.,* viscosity) of the slag.

Even if the slag is partly molten, it will not be able to flow into a coke-bed as illustrated by an ore particle being heated and reduced in Figure 5. The partly liquid slag will not flow into the coke bed until it is reduced down to the point where no solid MnO is present, where the slag viscosity will be at its minimum as indicated in Figure 6 (left figure). It must also be mentioned that in addition to slag viscosity being affected by solid MnO particles, the size of the coke particles will also affect the

Table II. Primary Slag From Various Commercial African, Australian and South-American Ores (Calculated From Ref. 1)

	Comilog MMA	Comilog MMD	Comilog MMR	Comilog MMS	Comilog Sinter	Asman 48	Amapa Sinter	Amapa Miudo 40	Mamatwan	Gloria	Groote Eylandt	CVRD sinter	Wessel 38 pct	Wessel 50 pct
MnO	85	78	84	80	86	85	79	79	68	69	84	81	79	86
SiO2	7	11	8	11	7	7	10	9	6	8	9	6	7	5
Al2O3	7	11	8	9	7	1	9	12	1	0	6	10	4	0
MgO	0	0	0	0	0	1	1	0	5	5	0	1	1	1
CaO	0	0	0	0	0	6	1	0	21	17	0	2	9	7
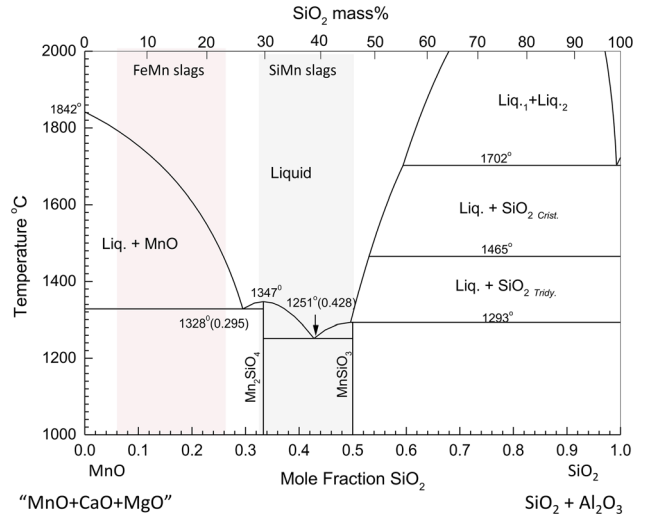
Fig. 3—MnO-SiO$_2$ phase diagram indicating the primary slag in FeMn and SiMn production, where MnO represents the basic oxides of MnO + CaO + MgO and SiO$_2$ represents the acid oxides such as SiO$_2$ + Al$_2$O$_3$.
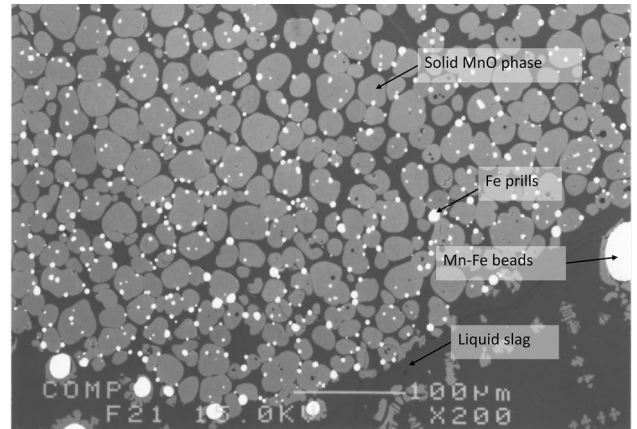

Fig. 4—Partly reduced FeMn slag containing solid MnO spheres in a liquid phase (adapted from Ref. 13).

flow of the slag into the coke bed as seen in Figure 6 (right picture) where the reduced slag is lingering on top of the coke particles.

The phase composition in slags from primary slag composition to tap-slag compositions may be illustrated with the ternary phase diagrams MnO-SiO$_2$-Al$_2$O$_3$ that represents the Comilog ore, Groote Eyland ore and the South-American ores, and the MnO-SiO$_2$-CaO diagram representing the South-African ores. While experimental work determining the slag phases exists,[22–24] we will in this paper use the FactSage databases to illustrate the reduction path, which equal the basicity line, as shown in Figure 7. There may of course be some deviations between experimental work and FactSage,[23] but the overall correlation is expected to be acceptable. From the Figure 7, the main reduction path seen in the binary MnO-SiO$_2$ phase diagram can be found. The high MnO ores will, when enough liquid phase is formed, start to reduce in a liquid + solid MnO phase area. As the
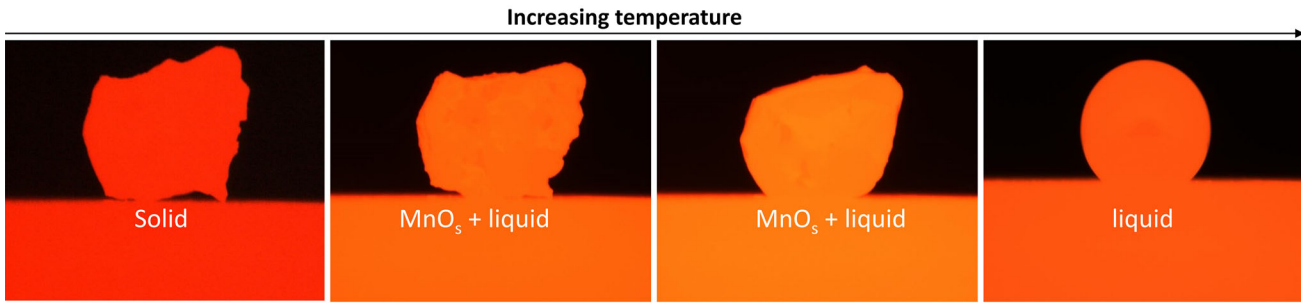
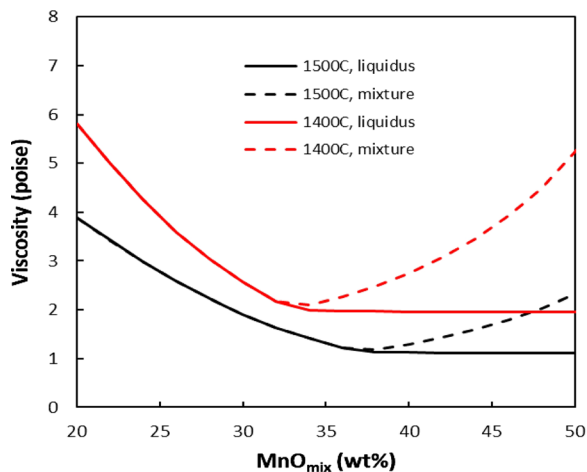Fig. 5—Mn-ore particle being heated in CO gas on a carbon substrate.

Fig. 6—FeMn-production: Slag viscosity during cooling adapted from Ref. 1 (left) and example of reduced slag from Comilog ore at 1600 °C[21] (right).

reduction proceeds to a lower MnO content, the solid MnO phase will gradually dissolve until the saturation composition is reached. It is also seen that this saturation compostion will be reached at a lower MnO content with higher basicities, which can also be seen in Figure 8. As mentioned above, the tap-slag is quite close to the saturation composition of around 30-40 pct MnO for a basicity of 0.7 and around 20 pct MnO at basicities of 1.1. This is believed to be due to the activity of MnO, and the effect the activity of MnO has on the reaction rate, as will be discussed later.

Depending on the mineralogy and distribution of minerals in the original ores, the raw materials will not always behave close to the equilibrium state given by the phase diagrams. A large effort has hence been done to find the melting behaviour of the ores under a certain heating rate with carbon present, that is when it starts to soften, also called initial melting, when it melts, and when it is completely molten (i.e the liquidus is obtained either due to a high temperature and/or to a low MnO content.[3,6,19,25–31]) These stages represent the steps an ore particle experiences in the Submerged Arc Furnace and are illustrated in Figure 5. While large variation exists in the results, the main trend is that more acid materials will produce a larger amount of liquid phase at a lower temperatures, in agreement with the phase diagrams already discussed. The materials will also produce a larger amount of liquid phase at low temperatures when it has been heat-treated at high temperatures. This can be explained by the basic and acid minerals mixed in an ore has dissolved into silicate phases when heat-treated and will hence melt at lower temperatures. To exemplify this according to Figure 3 for a constant heating rate: if a pre-reduced ore contains the two individual phases MnO, with a melting point above 1800 °C, and SiO_2, with a melting point above 1700 °C, it will start to behave as partly liquid material at higher temperatures, than a Mn_2SiO_4 phase that has a melting point of 1363 °C due to kinetic restraints. It is of course the time to reach equilibrium state that will increase, however in a furnace with a fixed heating rate, this will then happen at a higher temperature (Figure 9).

When it comes to the primary slag formation for SiMn production, the average composition will be in the green area in Figure 3, as quartz is also added to the charge mix. Many producers are also using tap-slag from the FeMn production as a raw material. Since this slag contains around 30-40 pct MnO, it will be molten already at around 1250 °C, in the same area as the average primary slag composition. Two hypotheses exist for the reduction step in SiMn furnaces:

1. The Mn-sources will dissolve the quartz first, and the reduction will hence be from the average charge composition, that is the average primary slag com-
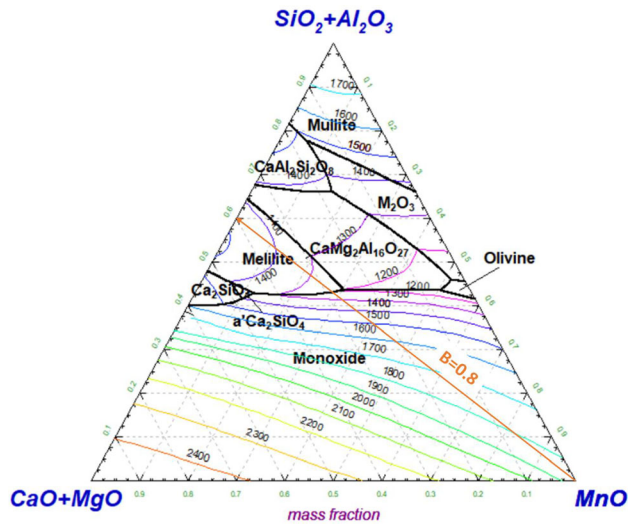
Fig. 7—Liquidus surface of MnO-SiO$_2$-Al$_2$O$_3$-CaO-MgO (A/S = 0.8, C/M = 7) slags calculated by FactSage software package. The basicity line of 0.8 is indicated.
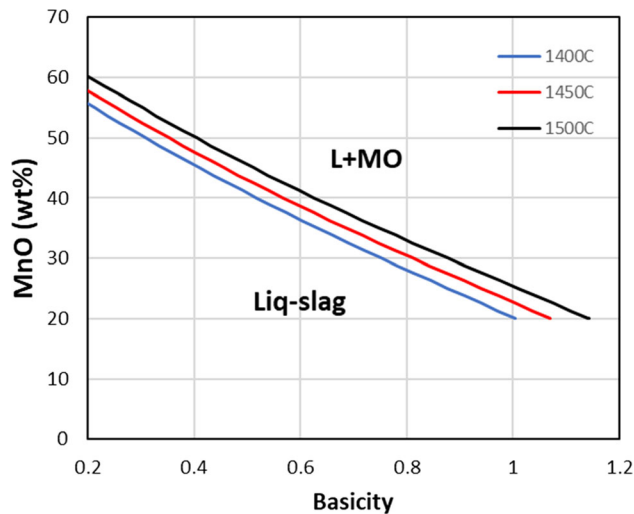

Fig. 8—Liquidus content of MnO *vs.* slag basicity in the MnO-SiO$_2$-CaO-Al$_2$O$_3$-5 pct MgO (Al$_2$O$_3$/SiO$_2$ = 0.57).

position. For quartz particles smaller than 2 cm it has been experimentally found that the quartz will dissolve in the Mn-source at temperatures less than 1400 °C, and that the reduction will not occur until around 1500 °C.[32–35] This step thus seems to hold for smaller quartz particles with good contact to the Mn-ore.

2. The reduction of Mn occurs from the partly molten Mn-source due to a slow quartz dissolution. The reduction of Si is thus determined by the quartz dissolution in the Mn-sources. Partly molten quartz has been found in the high temperature area in some industrial excavations, however it is rarely seen in pilot scale excavations. The dissolution of large quartz particles may hence be a larger problem for

the electric current paths in the furnace, than for the average slag reduction.

As the effect of dissolution rate of quartz is yet not agreed upon, one can mention that Maroufi *et al.*[36] investigated the quartz dissolution in a SiMn slag and found that the dissolution rate was determined by mass transfer of silica in the slag.

B. *High Temperature Thermodynamics*

The thermodynamics of the alloy-slag-gas-solid carbon system is investigated by a number of researchers like.[13,37–40] In the following, FactSage will be used to highlight the main issues regarding the thermodynamics in the FeMn and SiMn process.

In the two-phase reaction area in Figure 14, it can also be seen that the higher basicity has a slightly lower reduction rate than the lower basicity slags. As a higher basicity will have more solid MnO phase, and hence a higher viscosity, the mass transport of MnO in the slag may be contributing to the reduced reaction rate. It was however concluded that the chemical reaction was rate determining reaction as no MnO gradients was found in the liquid phase in the slag.[13,44] The effect on the reduction rate on the basicity is not yet fully understood. Both Ngoy[45] and Li[46] investigated Nchwaning and Comilog ores at various basicities from 0.04 to 1.3 by adding either quartz or lime to the ore. In the basicity area of 0.4-1, the effect of basicity was not seen. It was however seen that Comilog was reduced much faster than Nchwaning ore, for all basicities, and hence it is believed that the reduction rate may also be affected by trace elements as seen also for the reduction of SiMn slags.

The metal produced in the FeMn process is typically 78 pct Mn, 7 pct C, less than 1 pct Si and the rest is iron, typically ~ 14 pct (ASTM, grade B[41]). The equilibrium constant for reaction [1] can be expressed by equation.[3]

$$K = \frac{a_{Mn} \cdot p_{CO}}{a_{MnO} \cdot a_C} = \frac{a_{Mn} \cdot p_{CO}}{X_{MnO} \cdot \gamma_{MnO} \cdot a_C} \qquad [3]$$

where K is the equilibrium constant, a_{Mn} is the activity of Mn in the metal, p_{CO} is the partial pressure of CO in the gas phase, a_{MnO} is the activity of MnO in the slag, a_C is the activity of carbon, X_{MnO} is the mole fraction of MnO in slag and γ_{MnO} is the activity coefficient of MnO in the slag. As there is solid coke present, the activity of carbon is close to 1. The partial pressure of CO in equilibrium with solid carbon above 1200 °C is also close to 1, and as the metal composition is fixed at a fixed temperature, a_{Mn} is fixed. The amount of MnO in the slag can thus be determined by Eq. [4]. Evidently, the only variables affecting the MnO content in the slag is K and γ_{MnO}.

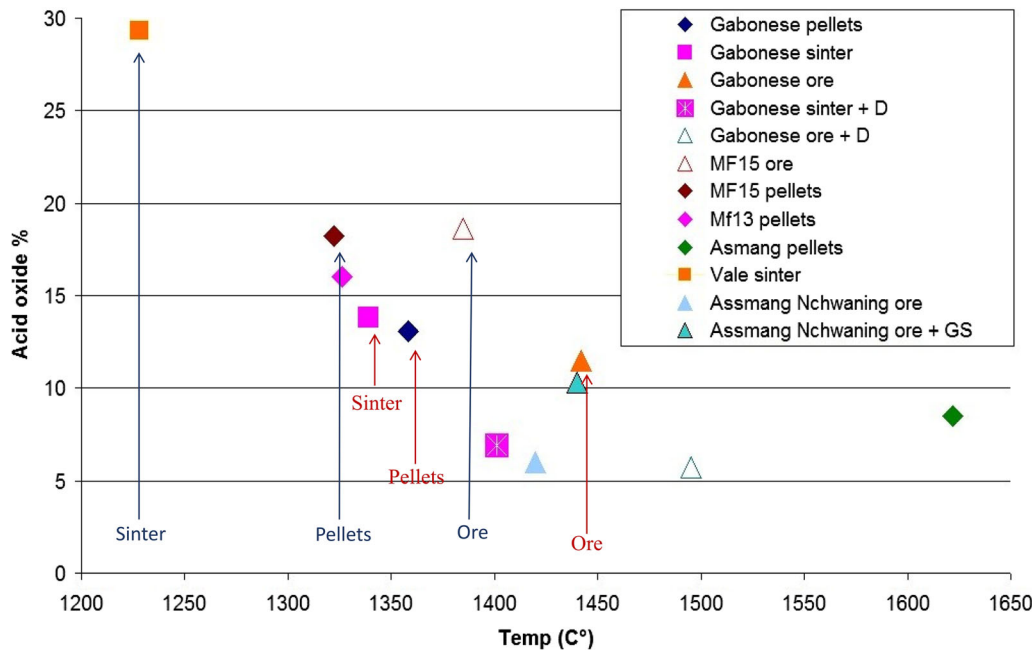$$X_{MnO} = \frac{1}{K} \cdot \frac{a_{Mn}}{\gamma_{MnO}} \qquad [4]$$

Fig. 9—Initial melting for various raw materials with various basicities and pre-treatment methods. Blue and red notation indicates the same ore with different pre-treatment (Color figure online) (adapted from Brynjulfsen 2013,[26] Ringdalen 2015[28]).

The practical aspects of Eq. [4] is that the MnO content in the slag will be determined by temperature, mainly through the equlibrium constant, and the slag composition, through the activity coefficient. The equlibrium constant is, as seen in Figure 10, strongly dependent on temperature, and hence a lower MnO content will be achieved at higher temperatures. The activity coefficient of MnO will increase with the basic oxides CaO and MgO, and decrease with the acid oxides SiO_2 and Al_2O_3. According to Gibbs phase rule one can then determine the MnO content as a function of basicity and temperature when two variables are fixed like e.g., the $Al_2O_3/SiO2$ ratio and pct MgO, as shown in Figure 11 for typical FeMn slags.

For SiMn slags, one needs to take into account reaction (2), that is the silicon distribution between the slag and the metal. Doing the same exercise as for the Mn distribution through Eqs. [5] and [6], it is seen that the silicon content in the metal is determined by the amount of SiO_2 in the slag, the temperature ($f(T)$, mainly given by the equilibrium constant), the other slag constituents, and the metal composition ($h(mc)$) as shown in Eq. [7]. The metal composition, that is the Mn/Fe ratio is not affecting the silicon content in the same manner as temperature and slag composition.[1] The correlation between the slag composition and temperature is shown in Figure 12. In order to obtain about 18 pct Si in the metal, the slag should be slightly below 40 pct SiO_2 at 1600 °C for a $(CaO + MgO)/Al_2O_3$ ratio of 1, which corresponding to most tapped slags. At low Al_2O_3 contents, i.e., a high $(CaO + MgO)/Al_2O_3$ ratio, a higher pct SiO_2 is needed to compensate for the lack of acid components.

$$K \ = \ \frac{a_{Si} \cdot p_{CO}^2}{a_{SiO_2} \cdot a_C^2} \ = \ \frac{X_{Si} \cdot \gamma_{Si} \cdot p_{CO}}{X_{SiO_2} \cdot \gamma_{SiO_2} \cdot a_C} \qquad [5]$$

$$X_{Si} \ = \ X_{SiO_2} \cdot K \cdot \gamma_{SiO_2} \cdot \frac{1}{\gamma_{Si}} \qquad [6]$$

$$Pct\, Si \ = \ pct\, SiO_2 \cdot f(T) \cdot g\left(\frac{pct\, CaO \ + \ pct\, MgO}{pct\, Al_2O_3}\right) \\ \cdot h(mc) \qquad [7]$$

The function $f()$ describes the temperature-dependent part, $g()$ the slag composition and $h()$ the metal composition. The MnO content in equilibrium with SiMn alloys is relatively low, as seen in Figure 13, typically around 10 pct at 1600 °C. This is quite low compared to what is typically tapped between 10-20 pct as discussed above.

C. Reaction Rates and Reduction Mechanism

The reduction mechanisms for FeMn and SiMn are quite different, and will in this part be discussed separately. For industrial conditions in Submerged Arc Furnaces, Mn has not been seen to be reduced in solid state more than a couple of percentages. This indicates that the major part of the reduction is occurring in liquid state. As discussed above, and illustrated in Figure 3, it means for FeMn primary slags, that the reduction will initiate in the two phase area of liquid phase and a solid MnO-phase. SiMn primary slag will
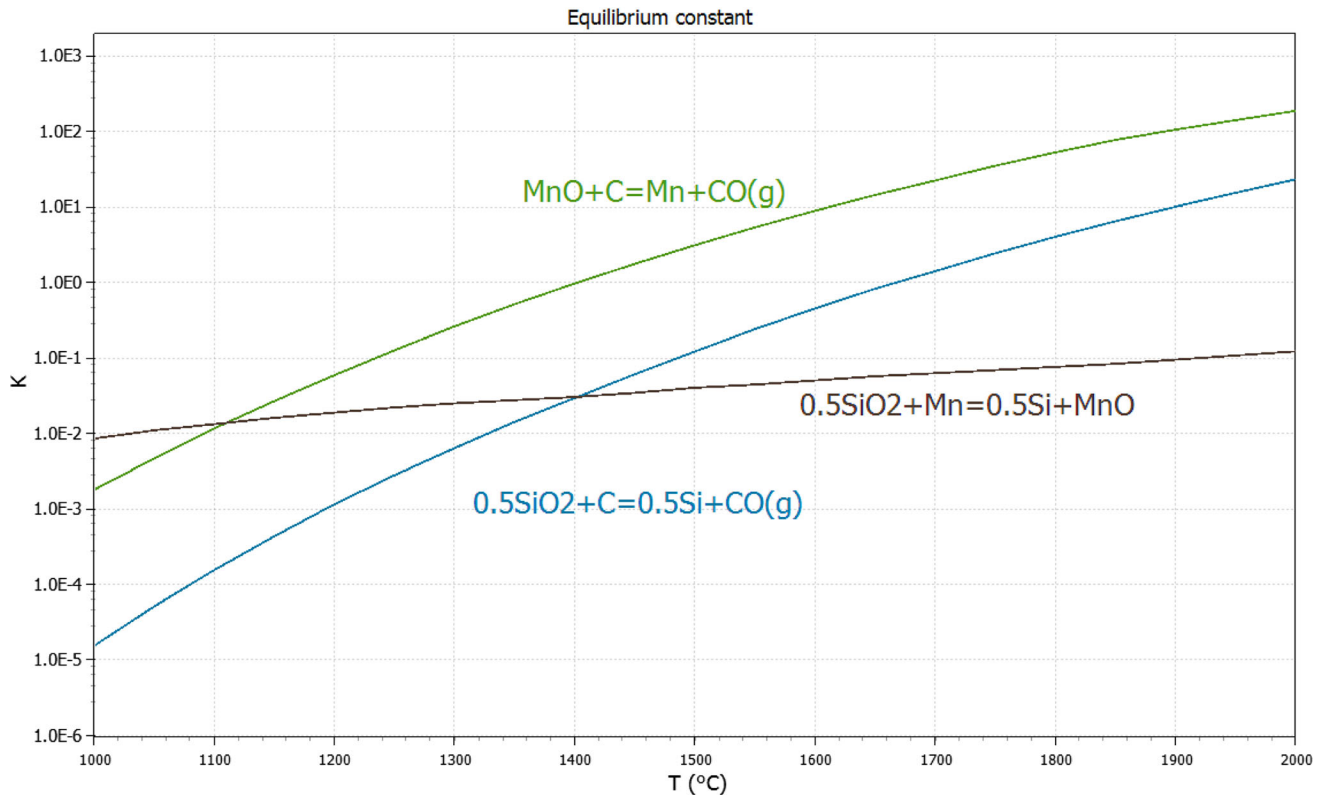
Fig. 10—Equilibrium constant of MnO and SiO$_2$ reduction according to reactions (1) and (2) (calculated from HSC Chemistry v.10).
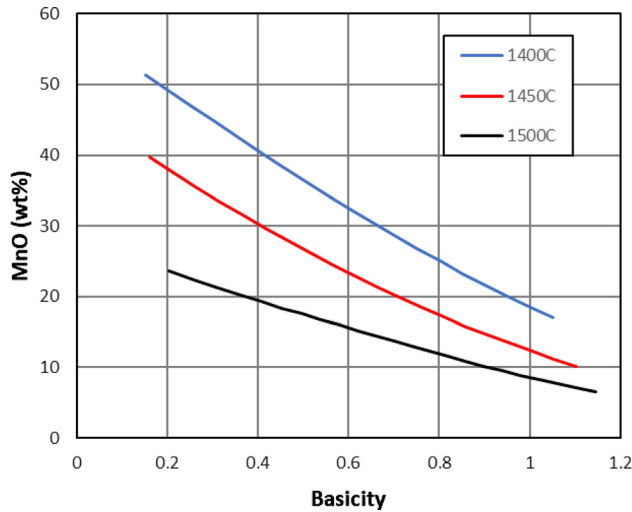

Fig. 11—MnO content *vs.* basicity for a Al$_2$O$_3$/SiO$_2$ ratio of 0.57 with 5 pct MgO in equilibrium with a FeMn where the Mn/Fe ratio is 7.8.

Fig. 12—Pct Si in the metal as a function of pct SiO$_2$ and temperature (for a fixed slag and metal composition)[1]. (Figure is reprinted with permission from Ref. 1).

probably be all liquid when the reduction starts. The mechanism during reduction will hence be affected by the phases in the primary slag.

The kinetics of a FeMn slag is described by a rapid reaction when the activity of MnO is high and close to 1 (above the liquidus composition) followed by a slow reaction step below the liquidus composition as the
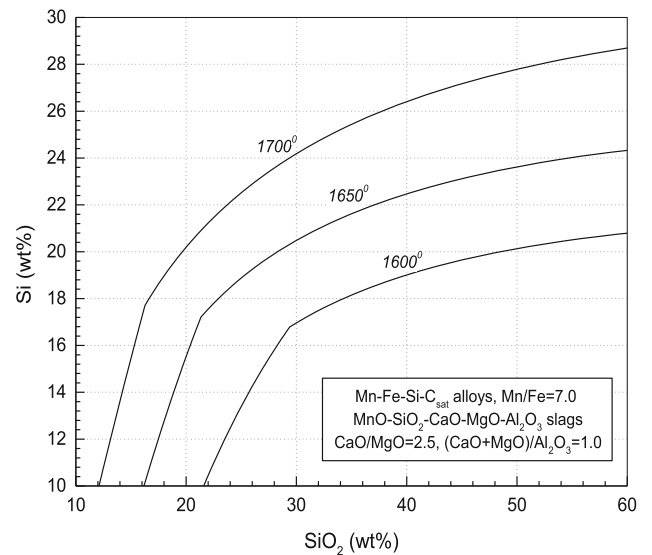
activity of MnO is drastically reduced, as shown in Figure 14. This is since the reaction rate will follow the activity of MnO according to reaction (8).

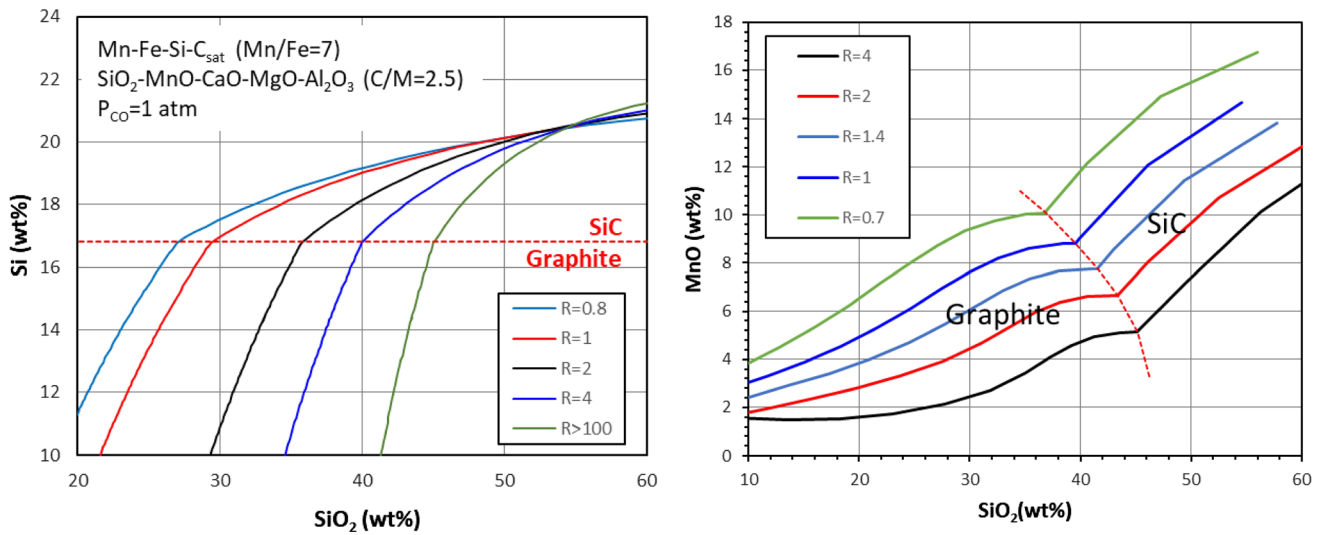$$\frac{d \text{ Pct MnO}}{dt} = A \cdot k \cdot \left(a_{\text{MnO}} - a_{\text{MnO(eq.)}} \right) \qquad [8]$$

Fig. 13—Pct Si in the metal and wt pct MnO in the slag as a function of slag composition for SiMn slags at 1600 °C. Slag composition is given by R = (CaO + MgO)/Al$_2$O$_3$.
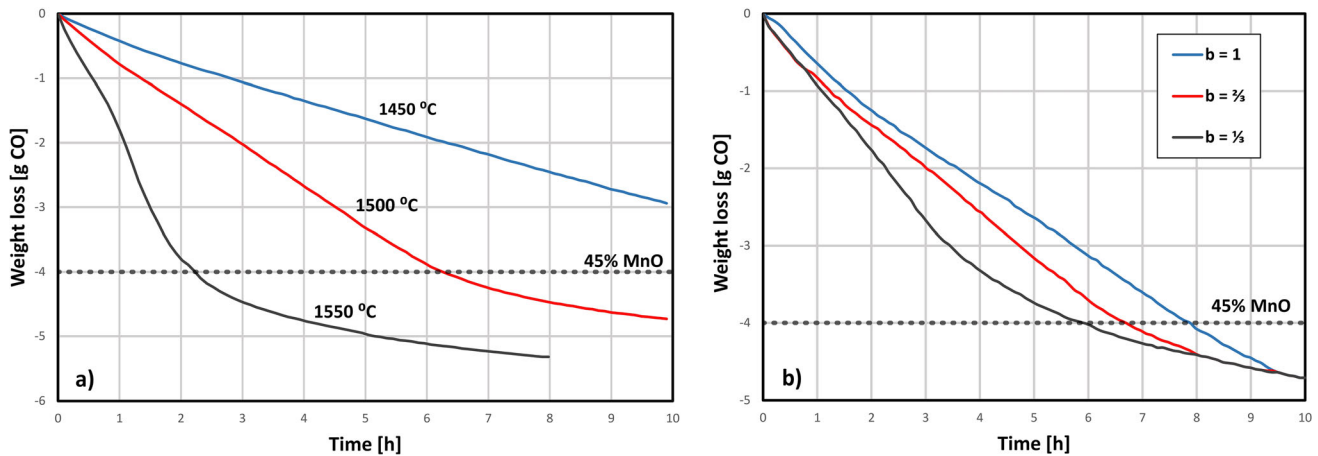

Fig. 14—Weight loss, representing the reaction rate of reaction (1) from 72 to 73 pct MnO with (a) Al$_2$O$_3$/SiO$_2$ ratio of 0.25 and basicity of 0.67 and (b) at 1500 °C and Al$_2$O$_3$/SiO$_2$ ratio of 0.5 (adapted from Ref. 40).
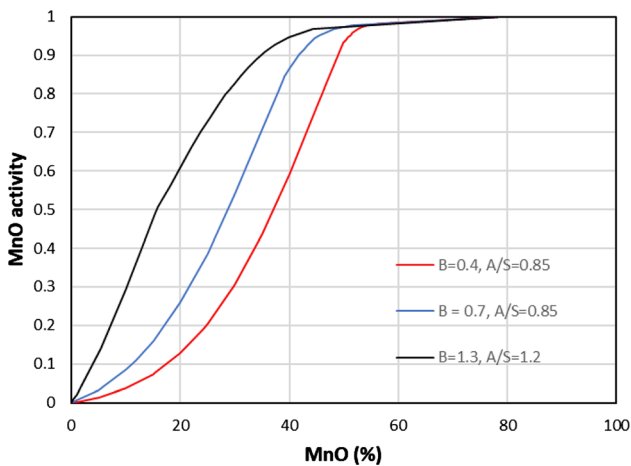

Fig. 15—MnO activity as a function of pct MnO at various basicities and Al$_2$O$_3$/SiO$_2$ ratios at 1500 °C.

where k is rate constant and A is the reaction area between the slag and the carbon material.[13,30,42] When the solid MnO phase is in equilibrium with the liquid slag, the activity of MnO is close to 1. Less than 20 pct MgO has been found to be present in the solid MnO phase[13] and according to Geldenhuis 43, the MnO activity in an MnO-MgO solid solution are ideal in this area. The activity will hence be high in the two-phase area, and when reaching the one phase liquid area, the reduction rate will decrease due to lower MnO activity. The MnO activity in the two and one phase area is shown in Figure 15.

The kinetics for the reduction of SiMn-slag is quite different. The reduction will occur while the slag is in liquid state above 1500 °C, above liquidus composition. It has previously been observed that sulfur in small amounts would increase the reaction rate, corresponding to iron in the metal.[47,48] This was in the later years verified by Referencs 32, 33, 49 through 51. The reaction rate will be very different when sulfur is present, as
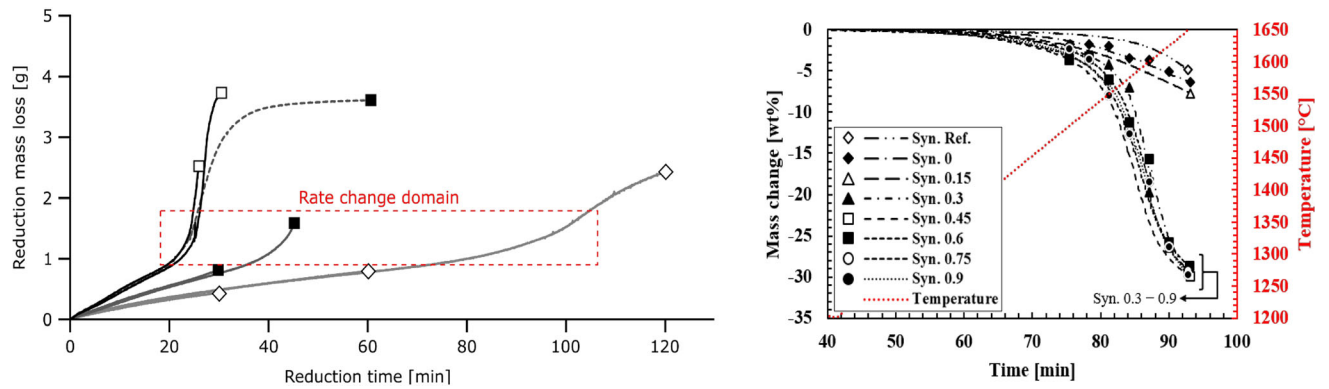
Fig. 16—Reduction rate of primary SiMn slag based on Assmang ore at 1540, 1610 and 1660°C (left figure)[50] and the reduction rate with varying S content (right figure), given as wt pct in the figure, at non-isothermal conditions.[55]

shown in the work from Tranell 52 and Hosum 53, where it was seen that the reaction rate was faster with charcoal compared to coke, when 0.3 pct S was present in the slag. When no slag was present, the coke would give a higher reaction rate, probably because of the high inherent S content in the coke.

In the SiMn reaction, the slag will initially react with a slow reduction step, followed by a fast reduction step as shown in Figure 16. Foaming has been observed in the slag after the initial step[33,50,53,54] and hence both a larger reduction area towards the coke as well as convection in the slag phase may increase the reduction rate. When enough sulfur was present ($\sim$ 0.3 pct S) it is seen that the first slow step, would hardly be present, and that the reduction would only go through the fast second step. The reaction rate for both MnO and SiO_2 can be calculated based on reaction (8).[50,55]

III. FUNDAMENTAL SLAG PROPERTIES IN THE FIVE COMPONENT MNO, MGO, CAO, SIO₂, AL₂O₃ SYSTEM

Numerous slag properties that are important for the Mn-ferroalloy productionare reviewed in this part of the paper. Specifically the slag structure, viscosity, density, surface- and interfacial tension and the electrical conductivity of the five-component slag system will be considered.

A. Slag Structure

The structure of silicate melts is of fundamental importance in metallurgical processes because the melt structure is closely linked to transport properties such as viscosity, density, and electrical conductivity.[56,57] The degree of polymerization (DOP) of silicate networks has been introduced as the most influential parameter for linking these properties and slag structure. DOP and viscosity are proportional, while density and electrical conductivities are inversely proportional to DOP.[58,59] In silicate slags, the presence of network-former and network-modifier elements determines the DOP of the silicate structure. SiO_2 is among the network-former

oxides, while alkali and alkali-earth oxides, such as Na_2O and CaO(basic oxides), contribute to depolymerization of the silicate network as network-modifying components. Amphoteric oxides, such as Al_2O_3, can act as either network-former or network-modifier oxide based on the availability of basic oxides in the silicate network.[60]

Other important parameters are oxygens species, namely bridging oxygen (O^0), non-bridging oxygen (O^-), and free oxygen (O^{2-}). In silicate networks, O^0 is connected to two network-former cations ($Si-O^0-Si$ or $Si-O^0-Al$), O^- is bounded to only one network-former cations ($Ca-O^--Si$), while O^{2-} is connected to only network-modifier cations ($Ca-O^{2-}-Ca$). By increasing O^{2-} through dissociation of basic oxides, the DOP of silicate networks decrease because O^{2-} reacts with O^0 in the silicates to split the highly complex structures of $Si-O$ into low polymerized units. There are various types of $Si-O$ units called Q^n species where n is the number of O^0 in the unit and can be 0 to 4. These units are monomer structure (Q^0), dimer structure (Q^1), chain structure (Q^2), sheet structure (Q^3), and 3-dimensional structure (Q^4).[61] The DOP parameter can be found both experimentally and theoretically through Q^n species obtained by Raman analysis and slag compositions, respectively. Oxygens species are also given experimentally using X-ray photoelectron spectroscopy (XPS) and theoretically using slag compositions.[62]

Raman spectroscopy has been employed to obtain information on the structural properties of various slags. So far, extensive research has been conducted on the silicate systems using Raman spectroscopy technique including the influence of basic and amphoteric oxides on the silicate structures.[61]

Although the five-component slag system MnO-SiO_2-CaO-MgO-Al_2O_3 has not been studied through Raman spectroscopic yet, there are several studies that have investigated slags containing MnO using Raman analysis.[58,59,63–66] Slag structure has been reported for the ternary systems of CaO-SiO_2-MnO[58,59,63] and MnO-SiO_2-Al_2O_3[66] as well as the quaternary systems of CaO-SiO_2-MnO-xCaF$_2$ [x = 0.0 to 14.5 wt pct],[63]
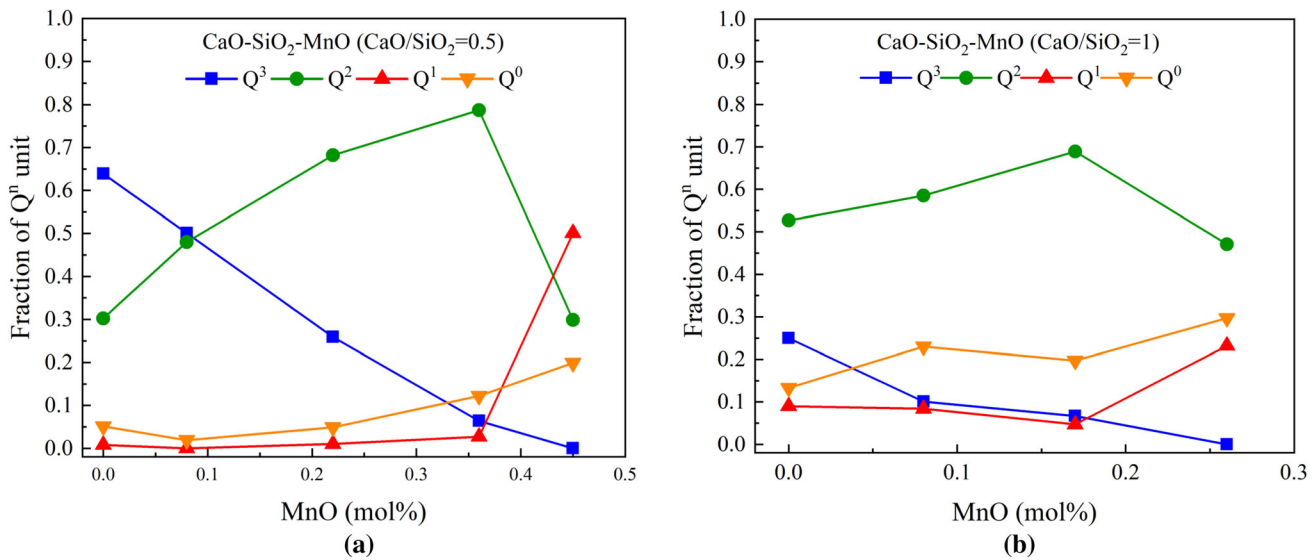
Fig. 17—Fraction of Q^n units *vs.* the MnO (mol pct) content. (*a*) the CaO-SiO$_2$-MnO (CaO/SiO$_2$ = 0.5) system and (*b*) the CaO-SiO$_2$-MnO (CaO/SiO$_2$ = 1) system (data from Ref. 58).
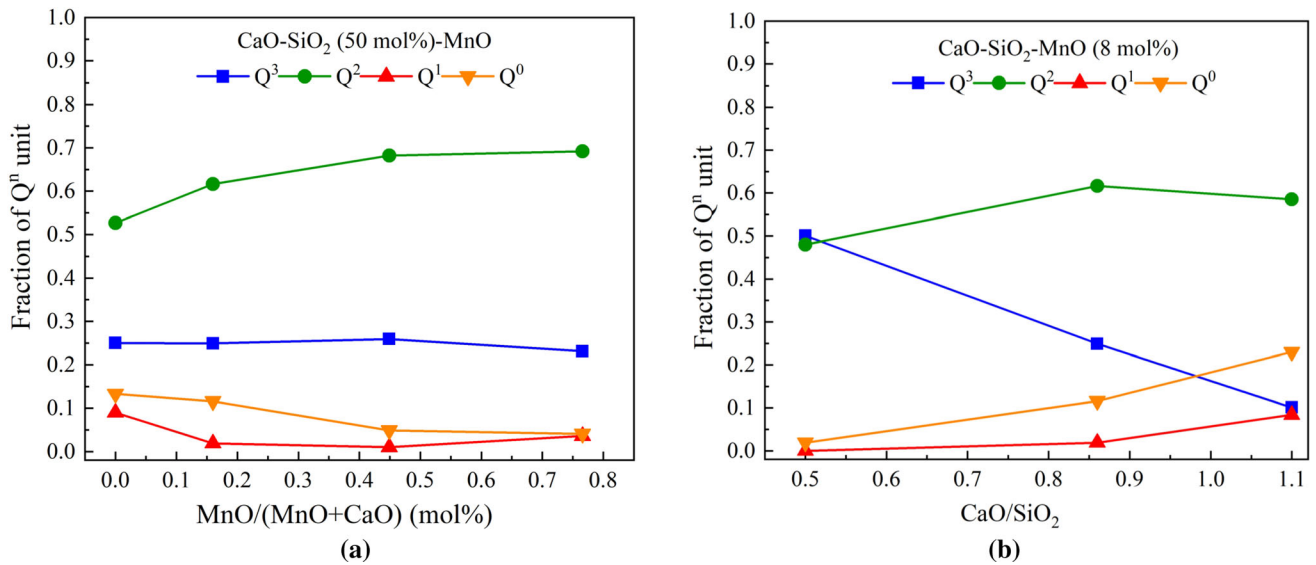

Fig. 18—(*a*) Fraction of Q^n units *vs.* the MnO/(MnO + CaO) (mol pct) content in the CaO-SiO$_2$ (50 mol pct)-MnO. (*b*) Fraction of Q^n units *vs.* the CaO/SiO$_2$ (mol pct) content in the CaO-SiO2-MnO (8 mol pct) (data from Ref. 58).

TiO$_2$-MnO (30 wt pct)-SiO$_2$-Al$_2$O$_3$,[64] MO-SiO$_2$-MnO-yCaF$_2$ [M(=Ca or Ba)O, y = 0 to 15 mol pct],[65] and MnO-SiO$_2$-Al$_2$O$_3$-zCe$_2$O$_3$ [z = 0.0 to 5.6 mol pct].[66]

Park[58] studied the structure of the CaO-SiO$_2$-MnO system using micro-Raman spectroscopic analysis quantitively. In this slag system, CaO, SiO$_2$, and MnO were varied from 0 to 52 mol pct, 36 to 63 mol pct, and 0 to 58 mol pct, respectively. The compositions containing around 10 to 20 and 40 to 50 mol pct MnO can be considered as simpler representatives of SiMn and FeMn slags, respectively. The variations of Q^n (Q^0 to Q^3) species were investigated with respect to MnO content, the substitution of CaO with MnO, and the ratio of CaO to SiO$_2$.

The influence of MnO addition was investigated for the CaO-SiO$_2$-MnO system at CaO/SiO$_2$ equal to 0.5 and 1.1 as shown in Figures 17(a) and (b), respectively. For both ratios of CaO/SiO$_2$, the variations of Q^0 to Q^3 showed similar behavior of increasing MnO. The Q^3 unit reduced and the fractions of Q^1 and Q^0 units increased continuously, while the fraction of Q^2 illustrated a maximum at around SiO$_2$ 40 mol pct.

Figure 18(a) presents the fractions of Q^n units with respect to the MnO/(MnO + CaO) changes in the CaO-SiO$_2$ (~ 50 mol pct)-MnO system. By the substitution of CaO by MnO, the Raman analysis found that the Q^3 unit slightly decreased while the Q^2 unit increased. The fractions of Q^1 and Q^0 units were slightly reduced by increasing MnO/(MnO + CaO). The effect of

CaO/SiO$_2$ changes on the slag structure was studied in the CaO-SiO$_2$-MnO (8 mol pct) system. Figure 18(b) displays the fractions of Q^n units *vs.* increasing CaO/SiO$_2$. The fraction of Q^3 unit was reduced while the fractions of Q^1 and Q^0 units were increased by increasing CaO/SiO$_2$ from 0.5 to 1.1, demonstrating that the depolymerization of the silicate network (or reducing DOP of the silicate structure) as the ratio of CaO to SiO$_2$ was increased at a fixed MnO content.

In this study, the Q^3/Q^2 ratio was proposed for determining DOP of the silicate network. The results shown in Figures 17 and 18 indicate that MnO is a network-modifier element in the silicate systems similarly to CaO, because the Q^3/Q^2 ratio reduced by increasing the MnO content, thereby the silicate network was depolymerized. Also, a linear correlation between ln (Q^3/Q^2) and viscosity, density, and electrical conductivity were explored, demonstrating the influence of slag structure (DOP of the slag network) on these slag properties. It was found that log viscosity increases linearly by increasing ln (Q^3/Q^2) while log density and log electrical conductivity reduce with increasing ln (Q^3/Q^2) linearly.[58]

B. Slag Viscosity

The viscosity of slag contributes to the metal-slag separation efficiency and tapping process, and is thus closely related to operation efficiency and minimizing the energy usage.[67] Slag viscosity depends on temperature and slag composition as the viscosity decreases with increasing temperature and basic oxide contents.

Viscosity measurements for the slag system MnO-SiO$_2$-CaO-MgO-Al$_2$O$_3$ have been carried out for various industrial applications.[68–71] A wide variation of slag compositions has been investigated which were close to slags in Mn-ferroalloy production in the submerged arc furnace. In addition to MnO-SiO$_2$-CaO-MgO-Al$_2$O$_3$, viscosity has been measured for its various subsystems such as the binary MnO-SiO$_2$ system,[72,73] the ternary systems of MnO-SiO$_2$-CaO[72,74,75] and MnO-SiO$_2$-Al$_2$O$_3$[73] as well as the quaternary systems of MnO-SiO$_2$-CaO-MgO[76] and MnO-SiO$_2$-CaO-Al$_2$O$_3$.[68,77] In general, the results of these investigations have revealed the effect of both temperature and MnO content. These findings suggest that slag viscosity decreases by increasing temperature and reduces by increasing the MnO content. The latter can be understood by considering the fact that MnO is a basic oxide and acts as a network breaker in the silicate network. In the following, some of the results and observations will be reviewed in more detail.

Viscosity measurements for MnO-SiO$_2$-CaO have been performed for a wide variety of compositions. In Segers et al. study,[72] the SiO$_2$ content was given as 32 to 50 wt pct while the contents of MnO and CaO were varied from 10 to 64 and 0 to 45 wt pct, respectively. The measurements were carried out at 1500 °C and illustrated the effect of SiO$_2$ and the substitution of CaO by MnO. In Ji's (2001) work,[75] SiO$_2$, MnO, and CaO were changed from 33 to 50 wt pct, 15 to 56 wt pct, and
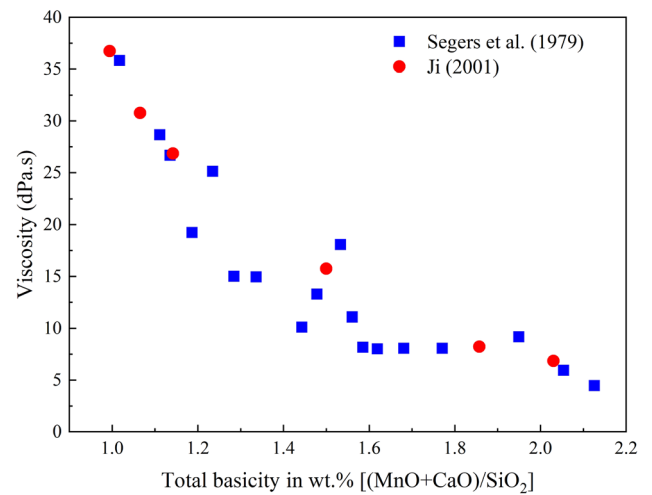

Fig. 19—Experimental viscosities (dPa.s) with respect to total basicity (wt pct) for the MnO-SiO$_2$-CaO system. Comparing results from Segers et al.[72] at 1500 °C and Ji[75] at 1480 °C.

8 to 45 wt pct. The viscosity measurements were reported for the temperature range from 1300 °C to 1480 °C. In Figure 19, the viscosity (dPa.s) is plotted as a function of the slag basicity (wt pct) introduced as (MnO + CaO)/SiO$_2$ for the MnO-SiO$_2$-CaO system to compare the results found by Segers et al.[72] at 1500 °C and Ji[75] at 1480 °C. As seen, the viscosity results of these two studies display the same trend, revealing that the viscosity reduces with increasing the basicity through increasing the basic oxides, namely MnO and CaO.

Woollacott et al.[69] reported the experimental viscosities at 1500 °C for a group of MnO-SiO$_2$-CaO-MgO-Al$_2$O$_3$ compositions related to slags in the production of high-carbon ferromanganese alloys. The MnO and SiO$_2$ contents were changed from 7 to 35 and 27 to 37 mol pct, respectively. Al$_2$O$_3$ was fixed at 10 mol pct, CaO and MgO were varied from 13 to 45 mol pct and 6 to 21 mol pct, respectively. It was found that SiO$_2$ content induces the major effect on viscosity. While an increase in the SiO$_2$ content increased the viscosity, MnO proved the strongest ability for reducing the viscosity among the involved basic oxides in the slag systems.

In another study published by Persson,[70] for slags associated with Mn-ferroalloy production in the submerged arc furnace, viscosity measurements were carried out within four groups of synthetic slags (called Slag A, B, C, and D) over wide composition ranges as presented in Table III. Each group includes compositions containing 30, 40, and 50 wt pct MnO, while SiO$_2$ and Al$_2$O$_3$ were varied from 14 to 33 and 8 to 33 wt pct respectively. CaO and MgO as basic oxides in the slag systems were changed from 4 to 29 and 0.3 to 7 wt pct, respectively. Table III displays the lower and higher measured temperatures which were limited by the presence of MnO precipitates and the use of alumina tube in the viscometer apparatus, respectively. The viscosities were measured over the temperature range from 1265 °C to 1712 °C where this range was varied based on the compositions.

Table III. Compositions (Wt Pct), Viscosity Measurements (dPa.s), and Temperature Ranges (°C) for Four Groups of Slags Associated With Mn-Ferroalloy Production (Data from Ref. 70)

| Slag name	MnO	SiO_2	CaO	Al_2O_3	MgO	Viscosity (dPa.s)	Temperature (°C)
A50	51.08	20.8	15.04	9.49	4.39	0.29–2.50	1321–1703
A40	40.8	25.29	18.21	11.34	5.25	0.38–2.86	1277–1706
A30	30.61	29.58	21.36	13.14	6.12	0.50–7.46	1265–1698
B50	50.69	14.38	10.63	24.65	0.35	0.34–4.48	1275–1696
B40	40.49	17.34	12.76	29.84	0.36	0.42–3.10	1355–1703
B30	31.47	20.19	14.99	33.15	0.62	0.66–4.55	1430–1712
C50	49.44	22.02	3.69	23.82	1.51	0.41–7.51	1284–1710
C40	39.96	27.2	4.49	27.33	1.83	0.77–6.47	1333–1703
C30	31.96	32.65	4.87	28.86	2.15	1.02–10.90	1368–1699
D50	50.84	15.62	21.13	8.09	4.94	0.23–0.56	1617–1695
D40	40.62	19.44	25.43	9.66	6	0.22–0.44	1449–1704
D30	32.14	22.07	28.69	11.44	6.65	0.31–0.65	1486–1694
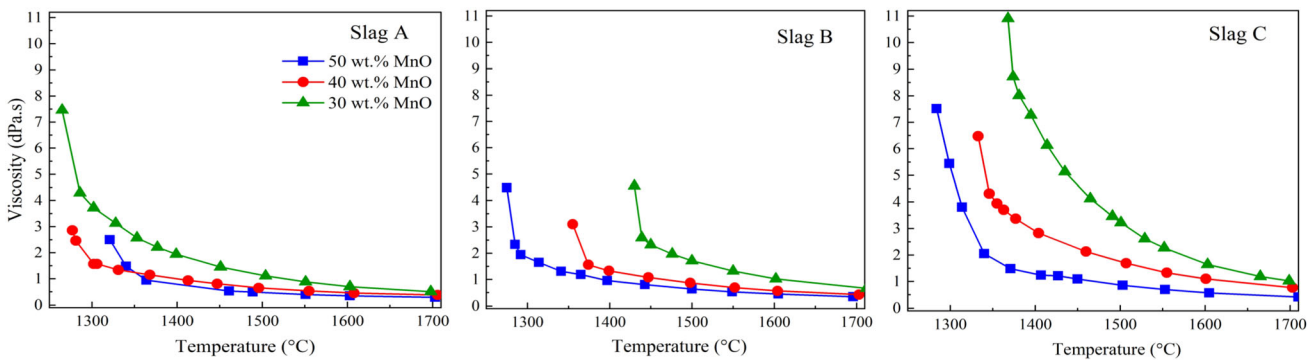
Fig. 20—Viscosity measurements (dPa.s) *vs.* temperature (°C) for Slag A, B, C, presented in Persson.[70]
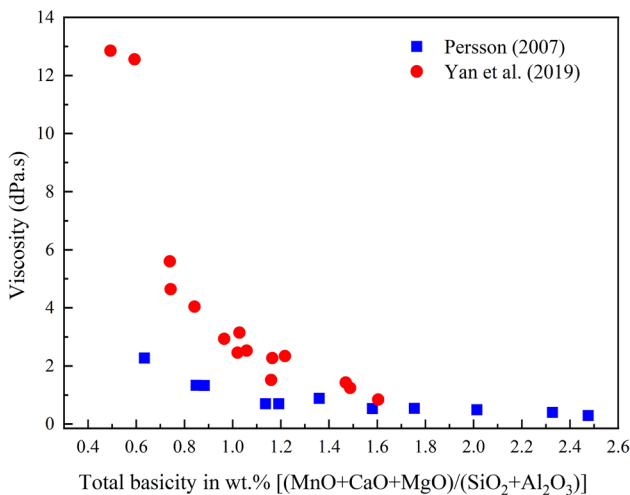

Fig. 21—Experimental viscosities (dPa.s) with respect to total basicity (wt pct) for the MnO-SiO₂-CaO-MgO-Al₂O₃ system. Comparing results from Persson 70 at 1550 °C to 1555 °C and Yan *et al.*[71] at 1550 °C.

Figure 20 shows the viscosity measurements (dPa s) with respect to the temperature (°C) for Slag A, B, and C. As expected, viscosities were decreased by increasing MnO from 30 to 50 wt pct for all slag groups.

Comparing the viscosities for slags containing the same amount of MnO suggested that slags with the highest amount of CaO possess the lowest viscosities, namely Slag D, while the highest viscosity values were reported for slags containing the highest amounts of SiO_2 and Al_2O_3, namely Slag C. It was also noted that the viscosity increases significantly below liquidus temperature because of the presence of solid particles. It is worth noting that MnO content further enhances the viscosity, due to higher amount of solid particles, compared to counterparts with a low amount of MnO, with smaller amount of solid particles.

Yan *et al.*[71] studied viscosity both experimentally and theoretically for the MnO (0 to 55 wt pct)-SiO_2-CaO-MgO (5 wt pct)-Al_2O_3 (20 wt pct) system in the temperature range from 1300 °C to 1600 °C. The SiO_2 and CaO contents were varied from 11 to 48 and 7 to 45 wt pct, respectively. The studied compositions were similar to the slags in FeMn- and SiMn-production. The results showed that the viscosity goes down by increasing MnO, specifically in melts with higher ratio of CaO to SiO_2.[71] The addition of 5 wt pct MnO increased the viscosities considerably for melts with the ratio of CaO to SiO_2 equal to 1.0 and 1.5, while the viscosity was only slightly reduced for the slag system with the ratio of CaO to SiO_2 equal to 0.6.

Table IV. Chemical Composition of Slags in FeMn and SiMn Production

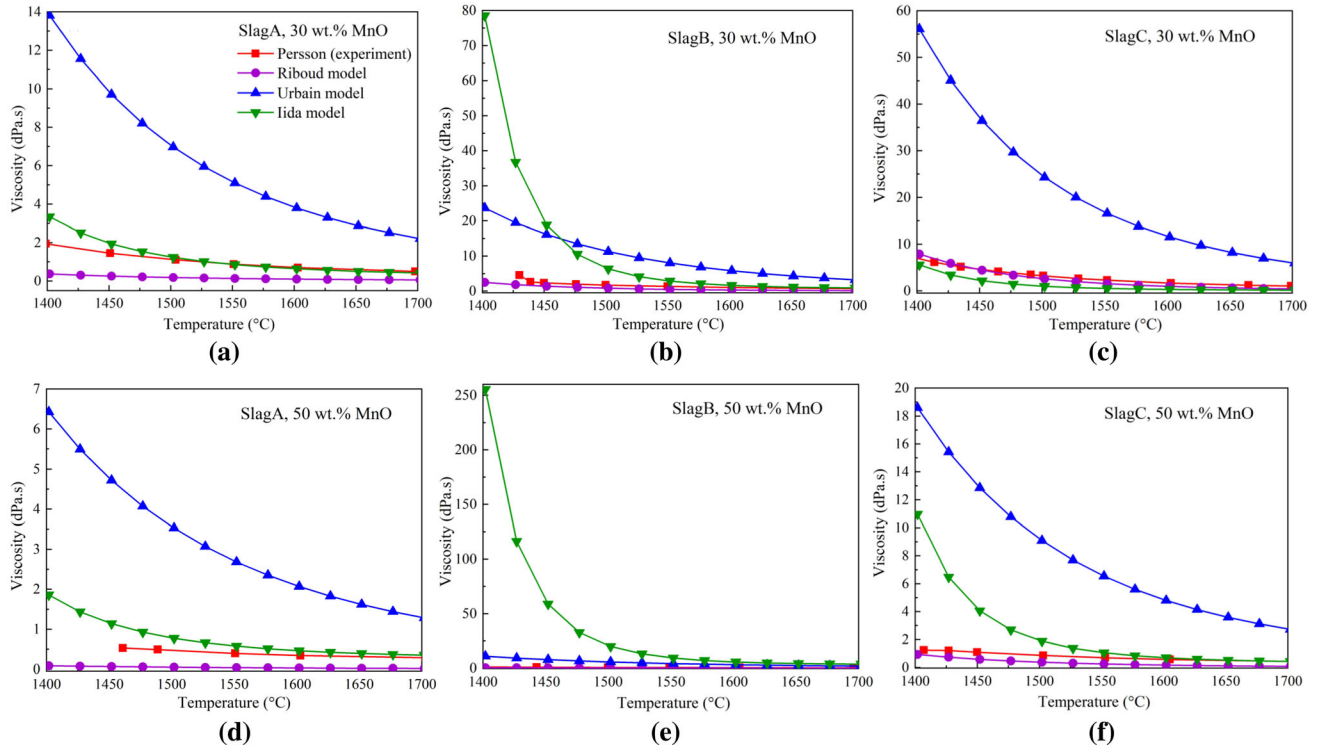| Slag	Chemical Composition (Wt Pct)					
	MnO	CaO	MgO	SiO$_2$	Al$_2$O$_3$	Other
High MnO-FeMn production[94]	28.0 to 30.0	28.0 to 30.0	6.0 to 6.5	28.0 to 30.0	5.0 to 5.5	1.0 to 1.3
Low MnO-SiMn production[95]	10.9	28.1	7.3	32.5	21.1	0.1

Fig. 22—Viscosity variations (dPa.s) *vs.* temperature (°C). Comparison of viscosities reported by Persson[70] with models from Riboud[84], Urbain[85], and Iida[86] for Slags A to C containing 30 and 50 wt pct MnO. (*a*) to (*f*) represents slag composition from Table III. (*a*) Slag A30, (*b*) Slag B30 (*c*) Slag C30, (*d*) Slag A50, (*e*) SlagB50 and (*f*) Slag C50.

Figure 21 exhibits the viscosity variations with respect to the total basicity (wt pct) defined as [(MnO + CaO + MgO)/(SiO$_2$ + Al$_2$O$_3$)] for data reported by Persson (2007)[70] at 1550 °C to 1555 °C and Yan *et al.*[71] at 1550 °C. As expected, the viscosity reduces by increasing the basicity in both studies, while the measured viscosity magnitudes by Yan *et al.* is larger than those viscosity values by Persson, specifically in lower basicities.

Although viscosity measurements have been performed on various slag systems, it is extremely challenging to produce experimental data for the entire range of compositions and temperatures. Furthermore, the high-temperature viscosity measurement is practically both time-consuming and high-cost. Accordingly, several models have been developed to predict slag viscosity for systems containing MnO.[71,74,76,78–83] The viscosity has been estimated for various binary, ternary, quaternary, and multicomponent systems. Comparing predicted viscosity values with experimental data has demonstrated that the models can provide reliable estimations of viscosity behavior with respect to both temperature and slag compositions.

In Figure 22, experimental viscosity results from Persson 70 are compared to the models proposed by Riboud 84, Urbain 85, and Iida 86 which depend only on slag compositions and temperature. It can be found that while the Urbain model overestimates the experimental data for all compositions presented, two other models predict better values especially the Iida model for the temperatures above 1550 °C. For slags in group B containing the lowest content of SiO$_2$ and highest content of Al$_2$O$_3$, the Iida model shows large variations with respect to temperatures lower than 1500 °C.
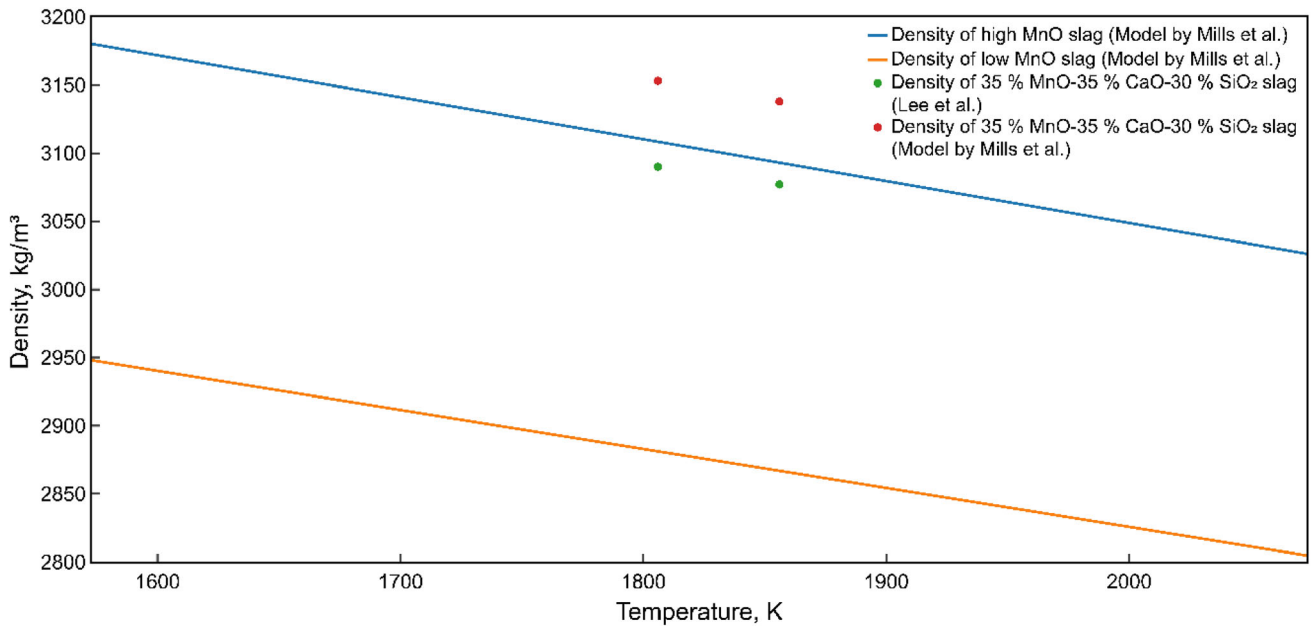
Fig. 23—Density of multicomponent MnO-containing slags. Composition of low and high MnO slags is shown in Table IV.

C. Density

There is a lack of density data on slags in Mn-ferroalloy production, but some insight may be gained by considering slags in steel production. Particularly, so-called mould slags in steel production consist of similar components as slags in Mn-ferroalloy production, MnO, CaO, MgO, SiO_2, Al_2O_3, while the main difference is the content of these components in both types of slags.[87]

In general, slag density can be determined by (a) numerical calculations based on previously established models[88] and (b) experimental methods, such as the sessile drop technique,[89] the Archimedes principle[90] or electrostatic levitation method.[91]

One of the most well-known numerical methods for calculating density of a multicomponent slag in liquid state is based on calculation of partial molar volumes,[88] which are expressed as:

$$V_{1773} = \sum_{i=1}^{N} X_i V_i$$

$$V_T = V_{1773} + 0.01(T - 1773 \text{ K})$$

[9]

where V_{1773} is slag partial molar volume of at 1773 K,[88,92] X_i is molar fraction of a component, V_i is partial molar volume of a component at 1773 K, V_T is slag partial molar volume at a certain temperature in liquid state and T is the certain temperature in liquid state.

Subsequently, density is defined as:

$$\rho_T = \frac{M}{V_T}$$

[10]

where ρ_T is density liquid state, M is mean molecular weight of all components in slag.

Figure 23 illustrates a comparison of the experimentally measured densities by Lee at al.93 and the calculated densities by the model from Mills et al.[2] for MnO-CaO-SiO_2-MgO-Al_2O_3 and MnO-CaO-SiO_2 slags. The density of MnO-CaO-SiO_2 slag estimated using the model shows fairly close values to those determined by Lee et al., and in addition, the calculated densities show the expected increase when MnO content is increased, which may indicate that the model of Mills et al. can be applied for slags in ferroalloy production with high reproducibility.

D. Surface and Interfacial Tension

Surface and interfacial tensions govern important phenomena such as wetting, foaming, refractory infiltration and slag-metal separation.[96–98] Interfacial behaviour depends upon the content of chemical elements and components interacting at the slag-metal interface, and thus interfacial tension changes as a function of slag composition. As with other properties of slags in ferroalloy production, there are few published data on surface tension of multicomponent slags and interfacial tension between slag and ferroalloys. However, studies on slags in steel production have shown that surface tension of most multicomponent slags lies in the range from 0.30 to 0.70 N/m.[99–101] Bublik et al.[102] have found that surface tension of slags corresponding to FeMn and SiMn production are 0.65 and 0.50 N/m, respectively.
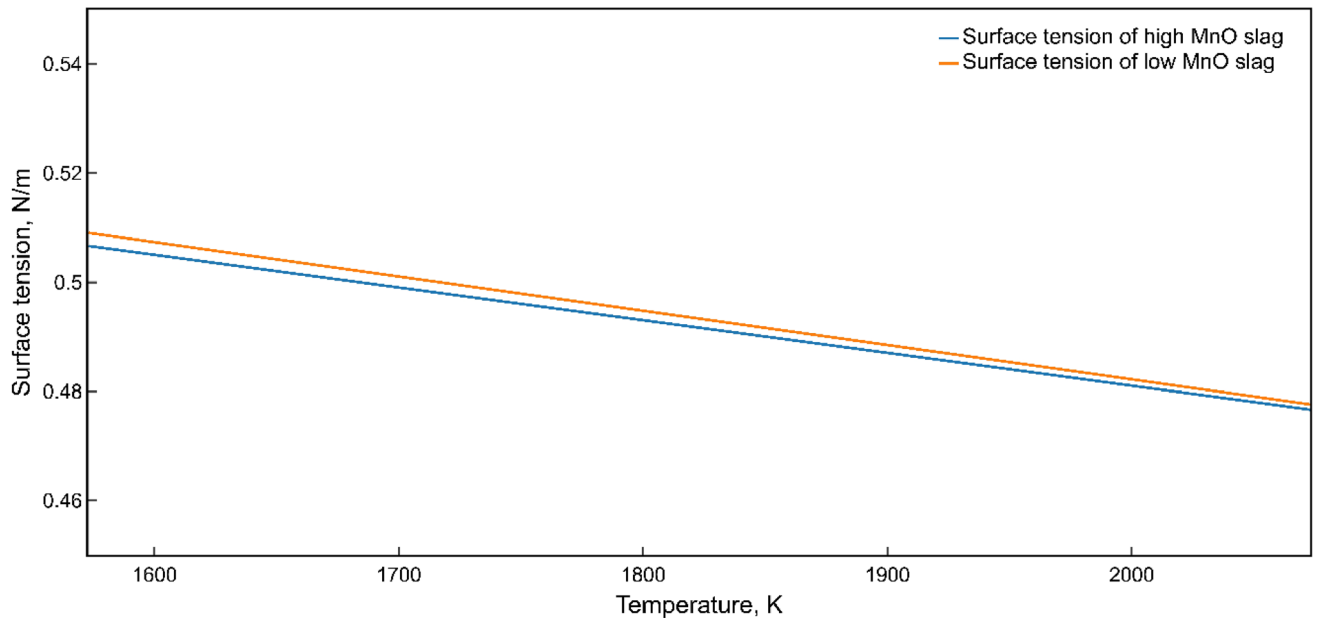
Fig. 24—Surface tension of high and low MnO slags. Composition of low- and high-MnO slags is shown in Table IV.
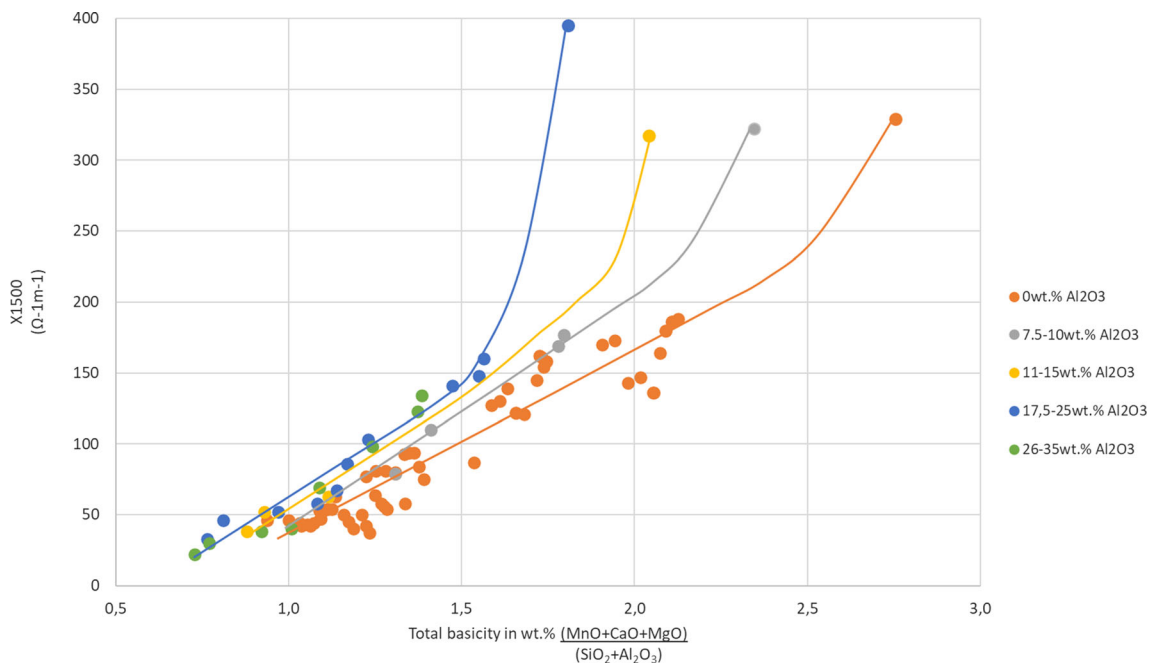

Fig. 25—Electrical conductivity *vs.* total basicity in wt pct for slags with various Al_2O_3 contents. The 4 non-linear points giving the electrical resistivity 250 S/m, are the slags with an MnO content above 65 wt pct [data used[108]].

Mills *et al.*[88] have reported that surface tension of multicomponent slags can be calculated assuming that surface tension is temperature-dependent and that all slag components modify surface tension depending on the mole fraction and their content in the bulk or at the surface. As such, Na_2O, K_2O, CaF_2 and B_2O_3 are treated as surfactants, while others as bulk components. Surface tension is then calculated using a system of equations:

$$\gamma_T = \gamma_{1773} + \frac{d\gamma}{dT}(T - 1773 \text{ K})$$

$$\gamma_{1773} = \left(\sum_{i=1}^{N} X_i \gamma_i\right)_{\text{bulk}} + \left(\sum_{i=1}^{N} X_i \gamma_i\right)_{\text{surf}} \quad [11]$$

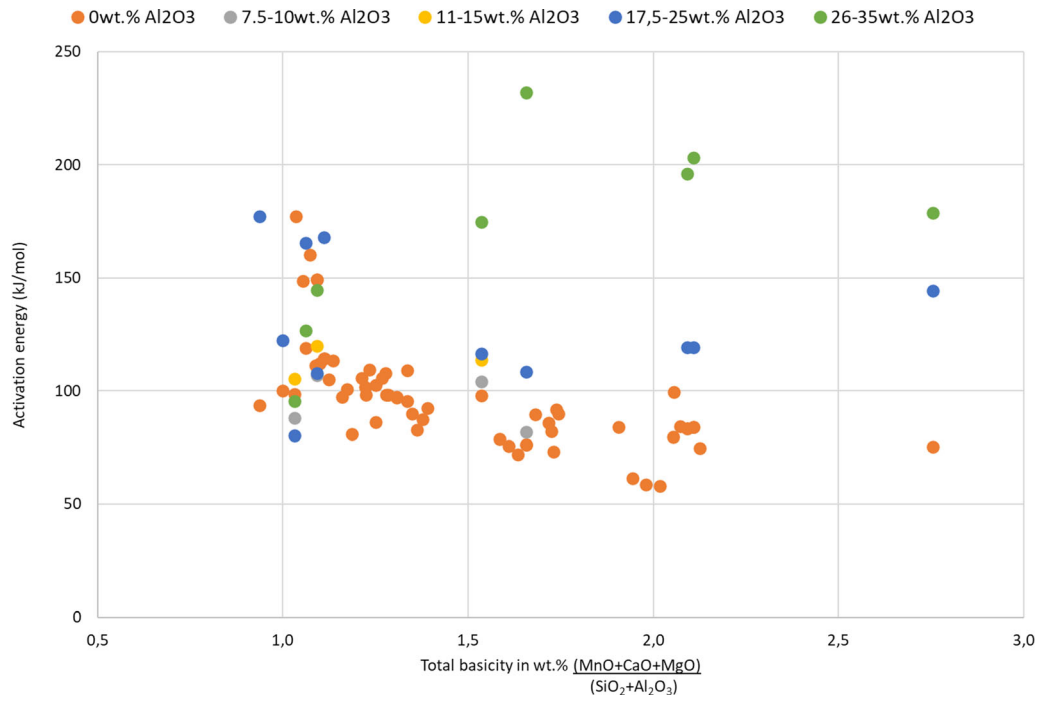$$\frac{d\gamma}{dT} = \sum_{i=1}^{N} X_i \frac{d\gamma_i}{dT}$$

Fig. 26—Activation energy of the conductivity of slags *vs.* total basicity in wt pct for slags with various Al_2O_3 content (data from Ref. 108).
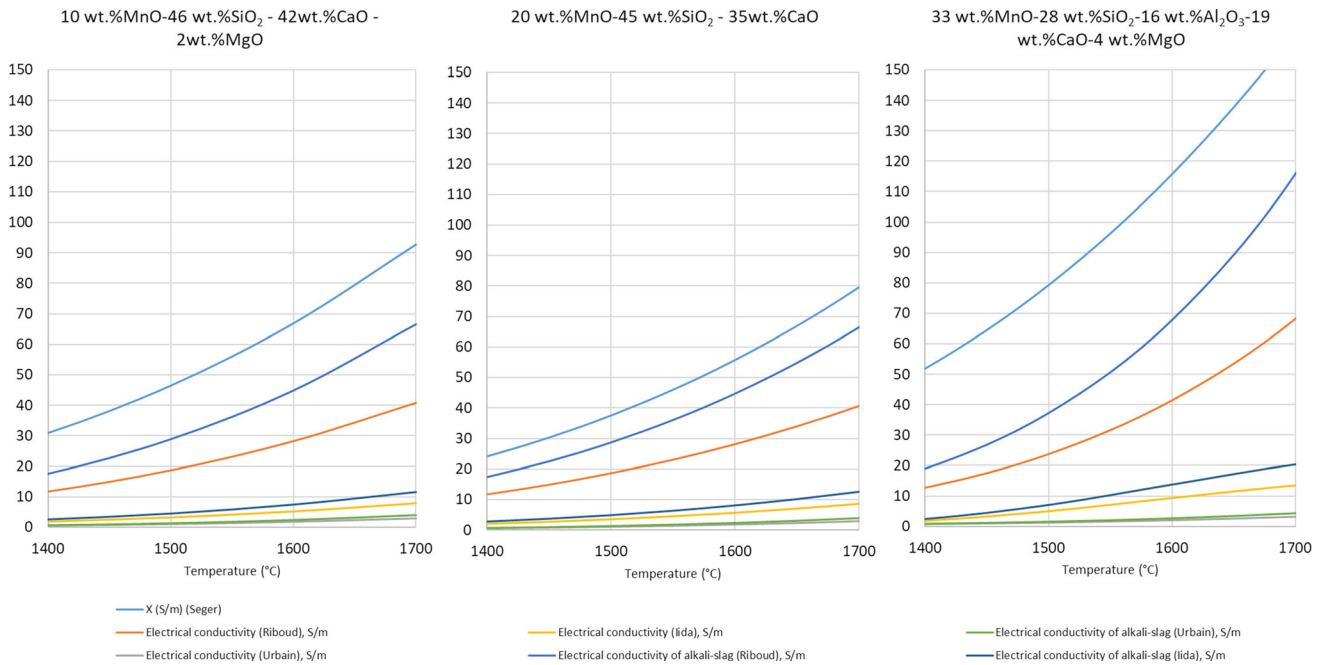

Fig. 27—Comparison of electrical conductivity (S/m) measured by Segers *et al.* with models from Riboud, Urbain and Iida of close to two SiMn slags and one FeMn slag. Though there are some differences, it is the alkali Riboud model that has the smallest deviation from the experimental data, followed by the Riboud model.

where γ_T and γ_{1773} are surface tension at a certain temperature and 1773 K, respectively.

Values of surface tension calculated using this model for slags as shown in Table IV is illustrated in Figure 24.

Sulfur and other surface-active elements have a significant influence on interfacial tension in liquid systems because they can affect the interfacial interaction at the slag-metal interface.[103–105] As a result, low interfacial tension leads to the formation of a slag-metal emulsion, metal droplet entrainment during tapping, and therefore poor slag-metal separation. Cramb et al.[106] have shown that interfacial tension between steel and slag sharply decreases with an increase of sulfur or oxygen activity. Bublik et al.[102] have suggested that higher sulfur content in ferroalloy-slag systems results in a higher mass transfer rate at the slag-metal interface, which again decreases both interfacial tension and apparent contact angle between slag and ferroalloys.

E. Electrical Conductivity

The electrical conductivity of slags in the steelmaking area, that is MgO, CaO, SiO_2 and Al_2O_3 has been investigated by several researchers and to mention one recent review on this system Wang et al.[107] can be mentioned. In the five component system including MnO, there is one main reference and that is Seger et al.[108] Seger and his group experimentally determined the slag from a basicity [$= (CaO + MgO)/(SiO_2 + Al_2O_3)$] from 0 to 0.93 and from 10 to 73 pct MnO, that is within the area of FeMn and SiMn production. The electrical conductivity at 1500 °C are shown in Figure 25. The tapping slags for FeMn and SiMn will typically be above 150 S/m and 40-120 S/m respectively. Overall, the electrical conductivity increases with basicity, and as the conductivity is shown as a function of the total basicity, including all 5 components, the conductivity of slags with higher alumina contents will be slightly higher, as alumina is less acid compared to silica. Most of the slags have a linear relationship between the total basicity and the conductivity, and the only exemption is the 4 points with higher than 65 wt pct MnO and no CaO and MgO, which shows conductivities higher than 300 S/m. It can however be mentioned that the $MnO/(CaO + MgO)$ ratio has no significant effect on the rest of the data.

The electrical conductivity is dependent on temperature and can be given by the Arrhenius equation where X (S/m) is conductivity, A is pre-exponential factor (S/m), E is activation energy in kJ/mol, R is gas constant (8.314 J/mol/K) and T is temperature (K):

$$X = A \cdot \exp\left(\frac{-E}{RT}\right) \qquad [12]$$

The activation energy, representing the temperature dependence of the conductivity of the slag, varies between 50-350 kJ/mol as can be seen in Figure 26. There is an indication that the activation energy of the low alumina slags decreases with basicity, while it increases for the high alumina slags.

As both the viscosity and the electrical conductivity is dependent on the slag structure, a correlation between the electrical conductivity and the viscosity has been proposed.[109] Based on the viscosity models of Riboud 110, Urbain 85 and Iida 86 one can hence calculate the electrical conductivity from slag composition and temperature, and in Figure 27 the experimental data from Segers et al. has been compared to the models. It can be seen that the experimental data are much higher compared to the models, however the Riboud alkali-model[109,110] gives the best fit.

CONFLICT OF INTEREST

On behalf of all authors, the corresponding author states that there is no conflict of interest.

REFERENCES

1. S. Olsen, M. Tangstad, and T. Lindstad: *Production of Manganese Ferroalloys*, Tapir, Trondheim, 2007.

2. D. Slizovskiy and M. Tangstad: Infacon, Helsinki, 2010.
3. D. Slizovskiy and M. Tangstad: Infacon, Almaty, Kazakhstan, 2013, pp. 185–94.
4. D. Slizovskiy: Doctoral Thesis, NTNU, Norway 2012.
5. M. Tangstad: *Handbook of Ferroalloys*, Elsevier, Amsterdam, 2013, pp. 221–66.
6. M. Tangstad, E. Ringdalen, E. Manilla, and D. Davila: in *7th International Symposium on High-Temperature Metallurgical Processing*, J.-Y. Hwang, T. Jiang, P.C. Pistorius, G.R.F. Alvear F., O. Yücel, L. Cai, B. Zhao, D. Gregurek, and V. Seshadri, eds., Springer, Cham, 2016, pp. 181–88.
7. M. Tangstad, P. Calvert, H. Brun, and A.G. Lindseth: Infacon, Cape Town, 2004, pp. 213–22.
8. H. Lagendijk, B. Xakalashe, T. Ligege, P. Ntikang, and K. Bisaka: Infacon, Helsinki, 2010, pp. 497–508.
9. M. Eissa, H. El-Faramawy, A. Ahmed, S. Nabil, and H. Halfa: *J. Miner. Mater. Charact. Eng.*, 2012, vol. 11, pp. 1–20.
10. T. Coetsee, C. Reinke, J. Nell, and P.C. Pistorius: *Metall. Mater. Trans. B*, 2015, vol. 46, pp. 2534–52.
11. M. Tangstad, E. Ringdalen, E. Manilla, and D. Davila: *JOM*, 2017, vol. 69, pp. 358–64.
12. N.A. Barcza, A. Koursaris, J.B. See, and W.A. Gericke: vol. 37, Iron & Steel Society of AIME, Detroit, 1979, pp. 19–33.
13. M. Tangstad: *PhD-thesis*, NTH, Norway, 1996.
14. M. Tangstad, B.Heiland, S.E.Olsen,R.Tronstad: INFACON, Canada, 2001, p. 6.
15. B. Monsen, M. Tangstad, and H. Midtgaard: Infacon,Cape Town, South Africa, 2004, pp. 392–404.
16. S.E. Olsen and M. Tangstad: Infacon, vol. 10, Cape Town, South Africa, 2004, pp. 231–38.
17. B. Monsen, M. Tangstad, I. Solheim, M. Syvertsen, R. Ishak, and H. Midtgaard: Infacon, vol. 11, The Indian Ferro Alloy Producers' Association, New Delhi, 2007, pp. 297–10.
18. E. Ringdalen and I. Solheim: *Infacon*, Southern African Institute of Mining and Metallurgy, Cape Town, 2018.
19. E. Ringdalen and M. Tangstad: Infacon, Almaty, Kazakhstan, 2013, pp. 195–206.
20. K. Tang and S.E. Olsen: *Infacon*, The Southern African Institute of Mining and Metallurgy, Cape Town, 2004.
21. D. Leroy: Master thesis, NTNU, Norway, 2007.
22. R. Rait and S.E. Olsen: Infacon, Helsinki, 2000.
23. E. Haccuria, P.C. Hayes, and E. Jak: *Int. J. Mater. Res.*, 2015, vol. 106, pp. 225–36.
24. B. Zhao, E. Jak, and P.C. Hayes: *ISIJ Int.*, 2006, vol. 46, pp. 1594–1602.
25. E. Ringdalen, M. Tangstad, and S. Gaal: in *Proceedings of the VIII International Conference on Molten Slags, Fluxes and Salts: 18 - 21 January 2009, Santiago, Chile*, M. Sanchez and Universidad de Concepción, eds., 1. ed., GECAMIN, Santiago, 2009.
26. T. Brynjulfsen and M. Tangstad: Infacon, Almaty, Kazakhstan, 2013, pp. 137–48.
27. M. Visser, H. Smith, E. Ringdalen, and M. Tangstad: Infacon in *MANGANESE FUNDAMENTALS*, Almaty, Kazakhstan, 2013, pp. 553–66.
28. E. Ringdalen, M. Tangstad, and T. Brynjulfsen: Infacon in *FUNDAMENTALS, THEORY*, Kiev, Ukraine, 2015.
29. B. Sorensen, S. Gaal, E. Ringdalen, M. Tangstad, R. Kononov, and O. Ostrovski: in *INFACON XII*, Helsinki, 2010, pp. 439–48.
30. T. Brynjulfsen and M. Tangstad: in *Characterization of Minerals, Metals, and Materials*, J.-Y. Hwang, S.N. Monteiro, C.-G. Bai, J. Carpenter, M. Cai, D. Firrao, and B.-G. Kim, eds., Wiley, Hoboken, NJ, 2012, pp. 147–54.
31. D. Slizovskiy, M. Tangstad, and S. Wasbø: unpublished research 2021.
32. P.P. Kim, J. Holtan, and M. Tangstad: in *Advances in Molten Slags, Fluxes, and Salts: Proceedings of the 10th International Conference on Molten Slags, Fluxes and Salts 2016*, R.G. Reddy, P. Chaubal, P.C. Pistorius, and U. Pal, eds., Springer, Cham, 2016, pp. 1285–92.
33. P.P. Kim and M. Tangstad: *Metall. Mater. Trans. B*, 2018, vol. 49B, pp. 1185–96.
34. J. Holtan: Master thesis, NTNU, Norway, 2016.
35. T.A. Larssen: Master thesis, NTNU, Norway, 2017.
36. S. Maroufi, G. Ciezki, S. Jahanshahi, S. Sun, and O. Ostrovski: *Metall. Mater. Trans. B*, 2015, vol. 46B, pp. 101–108.
37. D. Swinbourne, W.J. Rankin, and R.H. Eric: *Metall. Mater. Trans. B*, 1995, vol. 26B, pp. 59–65.
38. H. Cengizler and R.H. Eric: vol. 1, Southern African Institute of Mining and Metallurgy, Cape Town, South Africa, 1992, pp. 167–74.
39. A.L. Oklei, T.A. Chubnidize, and G.G. Arevadze: *J. Appl. Chem. USSR*, 1991, pp. 1565–68.
40. V. Olsø, M. Tangstad, and S.E. Olsen: Infacon, Beijing, China, 1998, pp. 279–83.
41. Y.E. Lee: *Encyclopedia of Materials: Science and Technology*, Elsevier, Amsterdam, 2001, pp. 3039–44.
42. O. Ostrovski, S.E. Olsen, M. Tangstad, and M. Yastreboff: *Can. Metall. Q.*, 2002, vol. 41, pp. 309–18.
43. J.M.A. Geldenhuis, E.B. Pretorius, and R.J. Dippenaar: The South African Institute of Mining and Metallurgy, Cape Town, 1992.
44. T. Brynjulfsen: Doctoral Thesis, NTNU, Norway 2013.
45. D. Mwana Bute Ngoy, M. Kalenga wa Kalenga, and M. Tangstad: *Metallurgist*, 2018, vol. 62, pp. 658–66.
46. X. Li, K. Tang, and M. Tangstad: *Minerals*, 2020, vol. 10, p. 97.
47. T.-A. Skjervheim: PhD, NTH, Norway, 1994.
48. B. Nadir: Master thesis, NTNU, Norway, 2015.
49. X. Li and M. Tangstad: *Metall. Mater. Trans. B*, 2019, vol. 50B, pp. 136–49.
50. V. Canaguier and M. Tangstad: *Metall. Mater. Trans. B*, 2020, vol. 51B, pp. 953–62.
51. P. Kim, T. Larssen, M. Tangstad, and R. Kawamoto: in *Applications of Process Engineering Principles in Materials Processing, Energy and Environmental Technologies*, S. Wang, M.L. Free, S. Alam, M. Zhang, and P.R. Taylor, eds., Springer, Cham, 2017, pp. 475–83.
52. G. Tranell, S. Gaal, D. Lu, M. Tangstad, and J. Safarian: Infacon,The Indian Ferro Alloy Producers' Association, New Delhi, 2007, pp. 231–40.
53. B.D. Hosum: Master thesis, NTNU, Norway, 2020.
54. V. Canaguier and M. Tangstad: *Metall. Mater. Trans. B*, 2020, vol. 51 (3), pp. 952–63.
55. P.P. Kim: Doctoral Thesis, NTNU, Norway, 2018.
56. B.O. Mysen, D. Virgo, and F.A. Seifert: *Rev. Geophys.*, 1982, vol. 20, p. 353.
57. K.C. Mills: *ISIJ Int.*, 1993, vol. 33, pp. 148–55.
58. J.H. Park: *ISIJ Int.*, 2012, vol. 52, pp. 1627–36.
59. J.H. Park: *J. Non-Cryst. Solids*, 2012, vol. 358, pp. 3096–102.
60. K.C. Mills, L. Yuan, Z. Li, G. Zhang, and K. Chou: *High Temp. Mater. Process.*, 2012, vol. 31, pp. 301–21.
61. B. Mysen and P. Richet: *Silicate Glasses and Melts*, Elsevier, Amsterdam, 2019, pp. 223–62.
62. I. Sohn and D.J. Min: *Steel Res. Int.*, 2012, vol. 83, pp. 611–630.
63. J.H. Park, K.Y. Ko, and T.S. Kim: *Metall. Mater. Trans. B*, 2015, vol. 46B, pp. 741–48.
64. J.B. Kim and I. Sohn: *ISIJ Int.*, 2014, vol. 54, pp. 2050–58.
65. T.S. Kim and J.H. Park: *J. Am. Ceram. Soc.*, 2019, vol. 102, pp. 4943–55.
66. T.S. Kim, S.J. Jeong, and J.H. Park: *Met. Mater. Int.*, 2020, vol. 26, pp. 1872–80.
67. C. Han: PhD Thesis, The University of Queensland, Australia, 2017.
68. I. Tanabe, K. Oku, and T. Honda: *J. Electrochem. Soc. Jpn.*, 1960, vol. 28, pp. E262–66.
69. L.C. Woolacott, D.D. Howat, and P.R. Jochens: South African Institute of Mining and Metallurgy, Johannesburg, South Africa, 1974, pp. 227–32.
70. M. Persson: PhD Thesis, Royal Institute of Technology, Sweden, 2007.
71. B. Yan, Y. Liu, Q. Shu, T. Deng, and B. Glaser: *Metall. Mater. Trans. B*, 2019, vol. 50B, pp. 376–84.
72. L. Segers, A. Fontana, and R. Winand: *Electrochim. Acta*, 1979, vol. 24, pp. 213–18.
73. G. Urbain, Y. Bottinga, and P. Richet: *Geochim. Cosmochim. Acta*, 1982, vol. 46, pp. 1061–72.
74. S. Sridhar, D. Sichen, S. Seetharaman, and K.C. Mills: *Steel Res.*, 2001, vol. 72, pp. 3–10.
75. F-.Z. Ji: *Metall. Mater. Trans. B*, 2001, vol. 32B, p. 181.
76. F-.Z. Ji, D. Sichen, and S. Seetharaman: *Int. J. Thermophys.*, 1999, vol. 20, pp. 309–23.

77. M. Kato and S. Minowa: *Trans. Iron Steel Inst. Jpn.*, 1969, vol. 9, pp. 31–38.
78. L. Zhang and S. Jahanshahi: *Metall. Mater. Trans. B*, 1998, vol. 29B, pp. 177–86.
79. S. Vargas, F.J. Frandsen, and K. Dam-Johansen: *Prog. Energy Combust. Sci.*, 2001, vol. 27, pp. 237–29.
80. K. Tang and M. Tangstad: vol. 11, Infacon, The Indian Ferro Alloy Producers' Association, New Delhi, 2007, pp. 345–57.
81. G-.H. Zhang, K-.C. Chou, Q-.G. Xue, and K.C. Mills: *Metall. Mater. Trans. B*, 2012, vol. 43B, pp. 64–72.
82. M.A. Duchesne, A.M. Bronsch, R.W. Hughes, and P.J. Masset: *Adv. Coal Sci. Technol. ICCST 2011*, 2013, vol. 114, pp. 38–43.
83. W-.Y. Kim, A. Pelton, C. Bale, E. Bélisle, and S. Decterov: *J. Miner. Metall. Sect. B*, 2013, vol. 49, pp. 323–37.
84. P.V. Riboud, Y. Roux, L.D. Lucas, and H. Gaye: *Fachber Huttenprax Met.*, 1981, vol. 19, pp. 859–69.
85. G. Urbain: *Steel Res.*, 1987, vol. 58, pp. 111–16.
86. T. Iida, H. Sakai, Y. Kita, and K. Shigeno: *ISIJ Int.*, 2000, vol. 40, pp. S110–14.
87. K.C. Mills and C-.Å. Däcker: *The Casting Powders Book*, Springer, Cham, 2017.
88. K.C. Mills, S. Karagadde, P.D. Lee, L. Yuan, and F. Shahbazian: *ISIJ Int.*, 2016, vol. 56, pp. 264–73.
89. M.A. Duchesne and R.W. Hughes: *Fuel*, 2017, vol. 188, pp. 173–81.
90. L. Muhmood and S. Seetharaman: *Metall. Mater. Trans. B*, 2010, vol. 41B, pp. 833–40.
91. T. Matsushita, T. Ishikawa, P-.F. Paradis, K. Mukai, and S. Seetharaman: *ISIJ Int.*, 2006, vol. 46, pp. 606–10.
92. K.C. Mills and B.J. Keene: *Int. Mater. Rev.*, 1987, vol. 32, pp. 1–120.
93. J. Lee, L.T. Hoai, J. Choe, and J.H. Park: *ISIJ Int.*, 2012, vol. 52, pp. 2145–48.
94. D. Groot, D. Kazadi, H. Pollman, J. Villiers, T. Redtmann, and J.D. Steenkamp: Infacon13, Almaty, Kazakstan, 2013.
95. E. Ringdalen, S. Gaal, M. Tangstad, and O. Ostrovski: *Metall. Mater. Trans. B*, 2010, vol. 41B, pp. 1220–29.
96. Y. Wanibe, H. Tsuchida, T. Fujisawa, and H. Sakao: *Trans. Iron Steel Inst. Jpn.*, 1983, vol. 23, pp. 322–30.
97. J. Wikström: PhD thesis, Royal Institute of Technology, Sweden, 2007.
98. R.A.M. de Almeida, D. Vieira, W.V. Bielefeldt, A.C.F. Vilela, R.A.M. de Almeida, D. Vieira, W.V. Bielefeldt, and A.C.F. Vilela: *Mater. Res.*, 2017, vol. 20, pp. 474–80.
99. J. Xin, N. Wang, M. Chen, and L. Gan: *ISIJ Int.*, 2019, vol. 59, pp. 759–67.
100. M. Hanao, T. Tanaka, M. Kawamoto, and K. Takatani: *ISIJ Int.*, 2007, vol. 47, pp. 935–39.
101. M. Wegener, L. Muhmood, S. Sun, and A.V. Deev: *Metall. Mater. Trans. B*, 2015, vol. 46B, pp. 316–27.
102. S. Bublik, S. Bao, M. Tangstad, and K.E. Einarsrud: *Metall. Mater. Trans. B*, 2021, vol. 52, pp. 2847–58.
103. L. Muhmood, N.N. Viswanathan, and S. Seetharaman: *Metall. Mater. Trans. B*, 2011, vol. 42B, pp. 460–70.
104. M. Suzuki, M. Nakamoto, T. Tanaka, Y. Tsukaguchi, K. Mishima, and M. Hanao: *ISIJ Int.*, 2020, vol. 60, pp. 2332–38.
105. T. Tanaka, H. Goto, M. Nakamoto, M. Suzuki, M. Hanao, M. Zeze, H. Yamamura, and T. Yoshikawa: *ISIJ Int.*, 2016, vol. 56, pp. 944–52.
106. A.W. Cramb and I. Jimbo: *Steel Res.*, 1989, vol. 60, pp. 157–65.
107. Y. Wang, L. Wang, and K-.C. Chou: *High Temp. Mater. Process.*, 2016, vol. 35, pp. 253–59.
108. L. Segers, A. Fontana, and R. Winand: *Can. Metall. Q.*, 1983, vol. 22, pp. 429–35.
109. K. Mills: Southern African Pyro Metallurgy, The Southern African Institute of Mining and Metallurgy, Johannesburg, 2011.
110. D. Kalisz: *Arch. Mater. Sci. Eng.*, 2012, vol. 58, pp. 164–70.